

Detailed electronic structure studies on superconducting MgB_2 and related compounds

P.Ravindran, P.Vajeeston, R.Vidya, A.Kjekshus and H.Fjellvåg

¹ *Department of Chemistry, University of Oslo, Box 1033, Blindern, N-0315, Oslo, Norway*
(October 24, 2018)

Abstract

Our recent electronic structure studies on series of transition metal diborides indicated that the electron phonon coupling constant is much smaller in these materials than in superconducting intermetallics. However experimental studies recently show an exceptionally large superconducting transition temperature of 40 K in MgB_2 . In order to understand the unexpected superconducting behavior of this compound we have made electronic structure calculations for MgB_2 and closely related systems. Our calculated Debye temperature from the elastic properties indicate that the average phonon frequency is very large in MgB_2 compared with other superconducting intermetallics and the exceptionally high T_c in this material can be explained through BCS mechanism only if phonon softening occurs or the phonon modes are highly anisotropic. We identified a doubly-degenerate quasi-two dimensional key-energy band in the vicinity of E_F along Γ -A direction of BZ (having equal amount of B p_x and p_y character) which play an important role in deciding the superconducting behavior of this material. Based on this result, we have searched for similar kinds of electronic feature in a series of isoelectronic compounds such as BeB_2 , CaB_2 , SrB_2 , LiBC and MgB_2C_2 and found that MgB_2C_2 is one potential material from the superconductivity point of view. We have also investigated closely related compound MgB_4 and found that its E_F is lying in a pseudogap with a negligibly small density of states at E_F which is not favorable for superconductivity. There are contradictory experimental results regarding the anisotropy in the elastic properties of MgB_2 ranging from isotropic, moderately anisotropic to highly anisotropic. In order to settle this issue we have calculated the single crystal elastic constants for MgB_2 by the accurate full-potential method and derived the directional dependent linear compressibility, Young's modulus, shear modulus and relevant elastic properties from these results. We have observed large anisotropy in the elastic properties consistent with recent high-pressure measurements. Our calculated polarized optical dielectric tensor shows highly anisotropic behavior even though it possesses isotropic transport property. MgB_2 possesses a mixed bonding character and this has been verified from density of states, charge density and

crystal orbital Hamiltonian population analyses.

I. INTRODUCTION

The recent discovery of superconductivity with high T_c ¹ in MgB₂ has initiated large activity in experimental as well as theoretical studies. Nb₃Ge is long been the record holder of the highest T_c among the intermetallic superconductors. The recently found YPd₂B₂C touches the same T_c as Nb₃Ge. The work of Bednorz and Müller² in 1986 on the basis of copper oxides started the discovery of a rapidly increasing number of high- T_c superconductors, among which the current record is held by HgBa₂Ca₂Cu₃O_{8- δ} with $T_c \sim 164$ K under pressure.³ During the past decade, remarkable progress in basic research and technological applications has been made on the high- T_c cuprate superconductors. However the complex crystal structures in combination with the multicomponent nature of the materials involved hinder the full understanding of microscopic origin of high- T_c superconductivity. Hence it may be beneficial to study the properties of a simple compound like MgB₂ in detail, which does not only have high T_c , but also takes a simple crystal structure with sp electrons (involved in the superconducting process) that are easy to handle theoretically.

In cuprates it is now generally believed that the conductivity takes place in the CuO₂ planes which, therefore, are essential to the high- T_c superconductors. The observation of superconductivity with high T_c in MgB₂ releases the question of whether superconductivity with even higher T_c can be found in intermetallics which do not comprise the characteristic CuO₂ planes. Several properties of MgB₂ appear closely related to high T_c superconducting cuprates: a low electron density of states, a layered structural character and the presence of rather light atoms (like oxygen in cuprates) facilitate high phonon frequencies. Further, although the electronic structure of this material has three-dimensional character, the B-B σ bands derived from B $p_{x,y}$ electrons (believed to be important for the superconductivity) reflect two-dimensional character. Like the cuprates, MgB₂ appears to exhibit hole conductivity, as evidenced from theoretical considerations⁴⁻⁷ and experimental Hall coefficient measurement.⁸ Another interesting aspect of the MgB₂ structure is that it has negatively charged honeycomb-shaped B planes which are reminiscent of highly negatively charged Cu-O planes in the high- T_c cuprates.

It is often believed that the d electrons play an important role for the superconducting behaviour of intermetallic compounds. So the experimental search for new superconductors has to a large extent been focussed on transition metal compounds. The back-ground for this is that transition metal compounds usually possess large density of states (DOS) at the Fermi level (one of the ingredients required for high T_c) than the main-group metal (sp) compounds. The BCS superconductors usually possess larger DOS at the Fermi level (E_F) and the high T_c in conventional superconductors is related to the large $N(E_F)$ values as well as the strong coupling of selected phonon modes to the electronic system. Further, relatively high T_c in superconducting intermetallics are believed to be coupled to a van Hove-like peak at E_F in the DOS curve, as predicted by various bandstructure calculations and indicated experimentally for Ni-site substituted rare-earth nickel borocarbides.⁹ However in MgB₂ there is no such peak-like feature at the vicinity of E_F in the DOS profile and hence one must search for some other origin of the superconductivity. MgB₂ is a sp metal and hence its value of $N(E_F)$ is small compared with that of superconducting transition metal compounds. Further, the presence of light borons in MgB₂ similar to oxygens in high- T_c cuprates, indicates that some exotic mechanism is involved in the superconduc-

tivity. On the other hand, theoretical studies⁷ show that the quasi two-dimensional B σ bands are strongly coupled with the E_{2g} phonon modes which would be consistent with the BCS mechanism. The experimentally observed isotope effect¹⁰ in MgB₂ also indicates phonon-mediated superconductivity. But, as discussed by Baskaran,¹¹ the absence of Hebel-Slichter peak in the NMR relaxation,^{12–14} a temperature dependent peak around 17 meV in the energy resolved neutron scattering,¹⁵ first order metal-to-metal transition on Al or C substitution,^{16–18} apparently anomalous temperature dependences of the Hall coefficient¹⁹ and London penetration depth²⁰ and the need of small μ^* value to explain the experimentally observed high T_c by the BCS theory²¹ indicate that the mechanism differs significantly from that of the BCS theory.

The discovery of new classes of quaternary intermetallic superconductors; the borocarbide^{22,23} and the boronitride²⁴ series, with relatively high T_c (up to 23 K for YPd₂B₂C²³) has encouraged the search for superconductivity in materials possessing light atoms such as B, C, N, H etc. Superconductivity with the T_c ranging 2–4 K has been observed for ternary transition metal diborides (YRe₂B₂, LuB₂C₂, YB₂C₂)^{25,26} and it is also observed in magnetic rare-earth (RE) rhodium borides (RERh₄B₄)²⁷. Very recently, the layer-structure compounds β -ZrNCl and β -HfNCl have been found to be superconducting upon Li intercalation with $T_c = 12.5$ and 25.5 K, respectively.²⁸ Another group of materials (maximum $T_c = 9.97$ K reported²⁹ for Y₂C₂I₂) is RE carbide halide superconductors with C–C pairs located in octahedrally coordinated voids of close-packed RE atoms. The recent discovery of superconductivity³⁰ at ≈ 14 K in the AlB₂-type phase of CaSi₂ (the highest T_c ever obtained among the silicides) indicates that the AlB₂-type structure may be favorable for superconductivity.

There are several mechanisms proposed for high T_c superconductivity in MgB₂ and the like. One is based on band structure findings,^{4,21} which suggests that the superconducting state results from strong electron-phonon interaction and high phonon frequency associated with the light boron atom. This is supported by the recent observation of relatively large boron isotope effect on T_c .¹⁰ A recent high-pressure study³¹ shows that T_c decreases with pressure at a rate of -1.11 K/GPa which is consistent with the BCS framework. It has been widely speculated that the low mass of boron is conducive for the occurrence of high phonon frequencies and consequently for high T_c . Another mechanism is called the "universal" by Hirsch⁵, and this conjectures that the superconductivity in MgB₂ (similar to that in cuprate superconductors) is driven by the pairing of the heavily dressed holes in bands that are almost full to gain enough kinetic energy to overcome the Coulomb repulsion. A positive pressure effect on T_c has also been predicted by Hirsch when the pressure reduces the interatomic B–B distance. An and Pickett⁷ maintain that the B σ bands are playing an important role in the superconductivity of MgB₂, and that the B in-plane E_{2g} phonon mode is strongly coupled to this band. Contradictory to the above viewpoint, Baskaran¹¹ concluded from the resonance valence bond (RVB) theory that the two dimensional σ bands do not play a crucial role in establishing high T_c superconductivity and $p\pi$ band might interfere with superconductivity.

MgB₂ possesses a hexagonal crystal structure and hence one can expect anisotropy in the physical properties of this material. Despite the strongly anisotropic layered hexagonal structure, its electronic properties indicate three dimensionality and the calculated Fermi velocity in the plane and perpendicular to the plane are almost the same. The theory for

hole superconductivity⁵ suggests that a decrease in the B-B interatomic distance should increase T_c . The RVB theory¹¹ suggests that a increase in chemical pressure along the c axis should decrease T_c and ultimately convert the material to a normal metallic state. In order to test these possibilities it is important to know the anisotropy in mechanical properties. From high-pressure total energy studies Loa and Syassen³² concluded that MgB_2 has isotropic compressibility. From a high-resolution x-ray powder diffraction high-pressure study along with the density functional calculation Vogt *et al.*³³ concluded that MgB_2 possesses nearly isotropic mechanical behavior. From isothermal compressibility measurements by synchrotron x-ray diffraction Prassides³⁴ concluded that MgB_2 is a stiff tightly-packed incompressible solid with only moderate bonding anisotropy between inter- and intralayer directions. However, Jorgensen *et al.*³⁵ found unusually large anisotropy in thermal expansion and compressibility from the neutron diffraction measurements. So, it is interesting to calculate the single-crystal elastic constants of MgB_2 to identify the exact nature of the anisotropy.

Several attempts have been made to enhance T_c by substitution of such as Al,¹⁶ Be,³⁶ Zn³⁷ and Li,³⁸ for Mg and C¹⁷ for B but no practical progress has hitherto been obtained. Moreover, the role of Mg and B site substitution on the electronic structure of MgB_2 has been studied theoretically.³⁹ So, it is interesting to search for compounds with an electronic structure similar to that of MgB_2 . A systematic investigation of this and related materials is a way to learn the mechanism of superconductivity in this novel material and to identify materials with high T_c . Knowledge of electronic structure, DOS, Debye temperature and related properties are important for assessing the mechanism and nature of superconductivity. In a search for superconducting diborides, BeB_2 is a promising candidate since the lighter Be may help to provide larger phonon frequencies and hence increase T_c . If the electron per atom ratio is important for the superconductivity in this class one should also consider CaB_2 and SrB_2 as interesting candidates. If it is the combination of Mg and B which brings the superconductivity in MgB_2 , one has to consider MgB_4 also. If the number of electrons in the B layers is a key for superconductivity in MgB_2 , related layer-structured materials such as LiBC , MgB_2C_2 should be paid attention. For these reasons we have made detailed electronic structure studies for the above mentioned compounds.

The rest of the paper is organized as follows. The structural aspects and the computational details about the calculations of the electronic structure, optical spectra and the elastic constants are given in in Sec. II. In Sec. III we have analyzed the bonding behavior of MgB_2 using the orbital and site projected DOS, crystal orbital overlap Hamiltonian population (COHP), charge density analysis etc. The electronic band structure of MgB_2 is calculated and compared with that of closely related systems and also analyzed the possible connection between the electronic structure and the superconductivity. The elastic and the optical anisotropy of this material are calculated and compared with available experimental results. Finally we summarize the important findings of the present study in Sec. IV.

II. STRUCTURAL ASPECTS AND COMPUTATIONAL DETAILS

A. Crystal structure details

MgB₂ (Fig. 1a) has AlB₂-type structure⁴⁰ with space group $P6/mmm$ and lattice parameters, $a = 3.084 \text{ \AA}$ and $c = 3.522 \text{ \AA}$. It is a simple hexagonal lattice of close-packed Mg layers alternating with graphite-like B layers, viz. B atoms arranged at the corners of a hexagon with three nearest neighbor B atoms in each plane. The Mg atoms are located at the center of the B hexagon, midway between adjacent B layers.

MgB₂C₂ crystallizes in an orthorhombic structure,⁴¹ space group $Cmca$ with $a = 10.92$, $b = 9.46$ and $c = 7.45 \text{ \AA}$. The structure of MgB₂C₂ (Fig. 1b) contains graphite-like but slightly puckered boron-carbon layers whose charge is counter-balanced by Mg²⁺ cations. The mutual coordination of boron and carbon consists of five atoms of the other kind, three of which being located in the same and two in adjacent layers. Each of Mg is coordinated by six B and six C atoms arranged at the corners of a slightly distorted hexagonal prism. The B-C distances within the layers range from 1.562 to 1.595 Å.

LiBC (Fig. 1c) crystallizes⁴² in a hexagonal primitive lattice with space group $P6_3/mmc$. The lattice parameters are $a = 2.752$ and $c = 7.058 \text{ \AA}$. The B and C atoms form a planar so-called heterographite layer. The interlayer regions are filled by Li. The B-C distance of 1.589 Å in LiBC is comparable with that in MgB₂C₂.

In MgB₄, the B atoms form interconnected pentagonal pyramids with the Mg atoms located in channels running parallel to the c axis. The Mg atoms form zig-zag chains. MgB₄ is orthorhombic, space group $Pnma$, with $a = 5.46$, $b = 7.47$ and $c = 4.42 \text{ \AA}$.⁴³ The average B-B distance in the pentagonal pyramid is 1.787 Å. Whenever possible we have used the experimental lattice parameters for our calculation, whereas for BeB₂, CaB₂ and SrB₂ we have used the optimized structural parameters obtained from total energy minimization.

B. Computation details for the FPLAPW calculations

These investigations are based on *ab initio* electronic structure calculations derived from density-functional theory. For the screened plasma frequency and the orbital projected DOS calculations we have applied the full-potential linearized-augmented plane wave (FPLAPW) method⁴⁴ in a scalar-relativistic version without spin-orbit (SO) coupling. In the calculation we have used atomic sphere radii 1.8 and 1.5 a.u. for Mg and B, respectively. The charge density and the potentials are expanded into lattice harmonics up to $\ell = 6$ inside the spheres and into a Fourier series in the interstitial region. The initial basis set included $3s$, $3p$ and $3d$ valence and $2s$, $2p$ semicore functions at the Mg site, $2s$, $2p$ and $3d$ valence functions for the B site. The set of basis functions was supplemented with local orbitals for additional flexibility in representing the semicore states and for relaxing the linearization errors generally. The effects of exchange and correlation are treated within the generalized-gradient-corrected local-density approximation using the parameterization scheme of Perdew *et al.*⁴⁵ To ensure convergence for the Brillouin zone (BZ) integration, 320 \mathbf{k} -points in the irreducible wedge of the first BZ of the hexagonal lattice for MgB₂ were used. Self-consistency was achieved by demanding the convergence of the total energy to be smaller than 10^{-5} Ry/cell. This corresponds to a convergence of the charge below 10^{-4} electrons/atom. For BeB₂, CaB₂ and SrB₂ we have made the structural optimization with the similar procedure.

C. Computation details for the TB-LMTO calculations

To calculate the electronic ground state properties of MgB_4 , MgB_2C_2 and LiBC we used the TB-LMTO method of Andersen.⁴⁶ The von Barth-Hedin parameterization is used for the exchange correlation potential within the local density approximation. In the present calculation, we used atomic sphere approximation. The calculations are semi-relativistic, i.e. except spin-orbit coupling, all other relativistic effects are included, taking also into account combined correction terms. BZ \mathbf{k} -point integrations are made using the tetrahedron method on a grid of 405 (MgB_4), 365 (MgB_2C_2) and 549 (LiBC) \mathbf{k} -points in the irreducible part of BZ. In order to have more insight into the chemical bonding, we have also evaluated the crystal orbital Hamiltonian population (COHP)^{47,48} in addition to the regular band structure calculations. COHP is the density of states weighted by the corresponding Hamiltonian matrix elements, a positive sign of which indicating bonding character and negative antibonding character.

D. Computational details of FPLMTO calculations

The full-potential LMTO calculations⁴⁹ presented in this paper are all electron, and no shape approximation to the charge density or potential has been used. The base geometry in this computational method consists of muffin-tin and interstitial parts. The basis set is comprised of augmented linear muffin-tin orbitals.⁵⁰ Inside the muffin-tin spheres the basis functions, charge density and potential are expanded in symmetry adapted spherical harmonic functions together with a radial function. Fourier series is used in the interstitial regions. In the present calculations the spherical-harmonic expansion of the charge density, potential and basis functions were carried out up to $\ell = 6$. The tails of the basis functions outside their parent spheres are linear combinations of Hankel or Neumann functions depending on the sign of the kinetic energy of the basis function in the interstitial regions. For the core-charge density, the Dirac equation is solved self-consistently, i.e., no frozen core approximation is used. The calculations are based on the generalized-gradient-corrected-density-functional theory as proposed by Perdew *et al.*⁴⁵ SO term is included directly in the Hamiltonian matrix elements for the part inside the muffin-tin spheres. Moreover, the present calculations make use of a so-called multi basis, to ensure a well converged wave function. This means that we use different Hankel or Neuman functions each attaching to its own radial function. This is important to obtain a reliable description of the higher lying unoccupied states, especially for the optical property studies. For our elastic properties study we have used 192 \mathbf{k} points and for the optical property studies 624 \mathbf{k} points in the irreducible part of BZ.

E. Calculation of optical properties

Once the energies $\epsilon_{\mathbf{k}n}$ and functions $|\mathbf{k}n\rangle$ for the n bands are obtained self consistently, the interband contribution to the imaginary part of the dielectric functions $\epsilon_2(\omega)$ can be calculated by summing the transitions from occupied to unoccupied states (with fixed \mathbf{k}

vector) over BZ, weighted with the appropriate matrix element for the probability of the transition. To be specific, the components of $\epsilon_2(\omega)$ are given by

$$\epsilon_2^{ij}(\omega) = \frac{Ve^2}{2\pi\hbar m^2\omega^2} \int d^3k \sum_{nn'} \langle \mathbf{k}n | p_i | \mathbf{k}n' \rangle \langle \mathbf{k}n' | p_j | \mathbf{k}n \rangle \times f_{\mathbf{k}n} (1 - f_{\mathbf{k}n'}) \delta(\epsilon_{\mathbf{k}n'} - \epsilon_{\mathbf{k}n} - \hbar\omega), \quad (1)$$

where $(p_x, p_y, p_z) = \mathbf{p}$ is the momentum operator and $f_{\mathbf{k}n}$ is the Fermi distribution. The evaluation of matrix elements in Eq. (1) is done over the muffin-tin and interstitial regions separately. Further details about the evaluation of matrix elements are given elsewhere.⁵¹ For hexagonal structure of MgB₂ the dielectric function is a tensor. By an appropriate choice of the principal axes we can diagonalized it and restrict our considerations to the diagonal matrix elements. We have calculated the two components $E||a$ and $E||c$ of the dielectric constants corresponding to the electric field parallel to the crystallographic axes a and c , respectively. These calculations yield the unbroadened functions. To reproduce the experimental conditions correctly, it is necessary to broaden the calculated spectra. The exact form of the broadening function is unknown, although comparison with measurements suggests that the broadening usually increases with increasing excitation energy. Also the instrumental resolution smears out many fine features. To simulate these effects the lifetime broadening was simulated by convoluting the absorptive part of the dielectric function with a Lorentzian, whose full width at half maximum (FWHM) is equal to $0.01(\hbar\omega)^2$ eV. The experimental resolution was simulated by broadening the final spectra with a Gaussian, where FWHM is equal to 0.02 eV. For metals, the intraband contribution to the optical dielectric tensor influence to the lower energy part of the spectra. This has been calculated using the screened plasma frequency obtained from Fermi surface integration with the description in Ref. 52.

F. Calculation of Elastic properties

The hexagonal phase of MgB₂ has two lattice parameters a and c with Bravais lattice vectors in matrix form

$$\mathbf{R} = \begin{pmatrix} \frac{\sqrt{3}}{2} & \frac{-1}{2} & 0 \\ 0 & 1 & 0 \\ 0 & 0 & \frac{c}{a} \end{pmatrix}.$$

The FPLMTO⁴⁹ method allows total-energy calculations to be done for arbitrary crystal structures. We can therefore apply small strains to the equilibrium lattice, then determine the resulting change in the total energy, and from this information deduce the elastic constants. The elastic constants are identified as proportional to the second-order coefficient in a polynomial fit of the total energy as a function of the distortion parameter δ .⁵³ We determine linear combinations of the elastic constants by straining the lattice vectors \mathbf{R} according to the relation $\mathbf{R}' = \mathbf{R}\mathbf{D}$. Here \mathbf{R}' is a matrix containing the components of the distorted lattice vectors and \mathbf{D} the symmetric distortion matrix, which contains the strain components. We shall consider only small lattice distortions in order to remain within the elastic limit of the crystal. In the following we shall briefly list the relevant formulas used to

obtain the elastic constants for hexagonal crystals. The internal energy of a crystal under strain, δ , can be Taylor expanded in powers of the strain tensor with respect to the initial internal energy of the unstrained crystal in the following way,

$$E(V, \delta) = E(V_0, 0) + V_0 \left(\sum_i \tau_i \xi_i \delta_i + \frac{1}{2} \sum_{ij} c_{ij} \delta_i \xi_i \delta_j \xi_j \right) + O(\delta^3) \quad (2)$$

The volume of the unstrained system is denoted V_0 , $E(V_0, 0)$ being the corresponding total energy. In the equation above, τ_i is an element in the stress tensor.

Since we have five independent elastic constants, we need five different strains to determine them. The five distortions used in the present investigation are described below. The first distortion

$$D_1 = \begin{pmatrix} 1 + \delta & 0 & 0 \\ 0 & 1 + \delta & 0 \\ 0 & 0 & 1 + \delta \end{pmatrix}$$

gives compression or expansion to the system. This preserves the symmetry but changes the volume. The strain energy associated with this distortion is

$$E(V, \delta) = E(V_0, 0) + V_0 [(\tau_1 + \tau_2 + \tau_3)\delta + \frac{1}{2}(2c_{11} + 2c_{12} + 4c_{13} + c_{33})\delta^2]$$

The second distortion

$$D_2 = \begin{pmatrix} (1 + \delta)^{-1/3} & 0 & 0 \\ 0 & (1 + \delta)^{-1/3} & 0 \\ 0 & 0 & (1 + \delta)^{2/3} \end{pmatrix}$$

gives volume and symmetry conserving variation of c/a . The energy associated with this distortion is

$$E(V, \delta) = E(V_0, 0) + V_0 [(\tau_1 + \tau_2 + \tau_3)\delta + \frac{1}{9}(c_{11} + c_{12} - 4c_{13} + 2c_{33})\delta^2]$$

The strain matrix

$$D_3 = \begin{pmatrix} \frac{1+\delta}{(1-\delta^2)^{1/3}} & 0 & 0 \\ 0 & \frac{1-\delta}{(1-\delta^2)^{1/3}} & 0 \\ 0 & 0 & \frac{1}{(1-\delta^2)^{1/3}} \end{pmatrix}$$

distorts the basal plane by elongation along a and compression along b in such a way that the volume is conserved. The energy associated with this distortion is

$$E(V, \delta) = E(V_0, 0) + V_0 [(\tau_1 - \tau_2)\delta + (c_{11} - c_{12})\delta^2]$$

The elastic constant c_{55} can be determined by the distortion of the lattice using the volume conserving triclinic distortion

$$D_4 = \begin{pmatrix} \frac{1}{(1-\delta^2)^{1/3}} & 0 & \frac{\delta}{(1-\delta^2)^{1/3}} \\ 0 & \frac{1}{(1-\delta^2)^{1/3}} & 0 \\ \frac{\delta}{(1-\delta^2)^{1/3}} & 0 & \frac{1}{(1-\delta^2)^{1/3}} \end{pmatrix}$$

The energy change associated with this distortion is

$$E(V, \delta) = E(V_0, 0) + V_0[\tau_5\delta + (2c_{55})\delta^2]$$

The fifth strain

$$D_5 = \begin{pmatrix} 1 & 0 & 0 \\ 0 & 1 & 0 \\ 0 & 0 & 1 + \delta \end{pmatrix}$$

involves stretching of the c axis while keeping other axes unchanged. Hence, the hexagonal symmetry is preserved but volume is changed. The energy change associated with this strain can be written as

$$E(V, \delta) = E(V_0, 0) + V_0[\tau_3\delta + (\frac{c_{33}}{2})\delta^2]$$

The elastic constant c_{33} can be directly obtained from the above relation. By solving the linear equations given above we have obtained all the five elastic constants. From pressure dependent lattice parameter measurements it is easy to obtain the bulk modulus along the crystallographic axes. Also to quantify the mechanical anisotropy of MgB₂ it is important to calculate the bulk modulus along the axes. For hexagonal crystals the bulk modulus along a (B_a) and c (B_c) are defined as

$$B_a = a \frac{dP}{da} = \frac{\Lambda}{1 + \alpha}$$

and

$$B_c = c \frac{dP}{dc} = \frac{B_a}{\alpha}$$

where $\Lambda = 2(c_{11} + c_{12}) + 4c_{13}\alpha + c_{33}\alpha^2$ and

$$\alpha = \frac{c_{11} + c_{12} - 2c_{13}}{c_{33} - c_{13}}$$

The calculated bulk modulus along the crystallographic axes obtained from these relations are compared with the experimental results in Sec. III.

III. RESULTS AND DISCUSSION

A. Electronic structure

The calculated electronic band structure of MgB₂ is given in Fig. 2. The interesting feature of this band structure is that a doubly degenerate, nearly flat, bands are present

just above the E_F in the Γ -A direction in Fig. 2 and cut the E_F along the K- Γ direction. These bands give rise to nearly cylindrical, hole-like Fermi surfaces around the Γ point,⁴ indicating that the transport properties are dominated by the hole carriers in the plane where B atoms exist. These bands are incompletely filled bonding σ bands with predominantly boron $p_{x,y}$ character. The p_z bands (they are mainly in the unoccupied state and having finite contribution along M- Γ direction at the VB in Fig. 2) are derived from the intralayer π bonding orbitals which also have interlayer couplings between adjacent atomic orbitals in the c direction. Our earlier study⁵⁴ on superconducting La_3X ($\text{X} = \text{Al, Ga, In, Tl}$) compounds show that the presence of a flat band in the vicinity of E_F gives large T_c (For La_3In addition of carbon gives a stable La_3InC compound for which E_F is brought to the pseudogap and results in a non-superconducting state.) The flat band feature is also present in the recently discovered superconducting $\text{YNi}_2\text{B}_2\text{C}$ compound. As a working hypothesis, we believe that this flat-band feature plays an important role for the superconductivity in MgB_2 . It is worth to recall that the calculated²¹ electron-phonon interaction strength also shows a large value in the Γ -A direction where the flat-band feature is seen. Moreover, zone boundary phonon calculations show that this band feature is very sensitive to the E_{2g} mode (B-bond stretching). We observed that the top of this flat-band feature is around 0.54 eV above E_F . Our calculations show that addition of around 0.32 electron to MgB_2 will bring E_F to the top of this energy band (assuming rigid band filling). Thus, if electrons are responsible for the superconductivity one can expect enhancement of T_c on electron doping. Slusky *et al.*¹⁶ have reported the role of electron doping on the superconductivity in $\text{Mg}_{1-x}\text{Al}_x\text{B}_2$ phase for which it is found that the T_c drops smoothly up to $x = 0.1$ and beyond $x = 0.25$ the superconductivity is completely destroyed. This indicates that holes are responsible for the superconductivity in MgB_2 an observation consistent with Hall effect measurements.⁸ The electron per atom ratio for TiB_2 is similar to that for MgB_2 and hence it seems worthwhile to make comparison between these phases. The electronic structure of TiB_2 ⁵⁵ shows that E_F is located in a pseudogap on the DOS curve and hence the estimated electron-phonon coupling constant is much smaller than for superconducting materials. This observation is consistent with the experimental findings in the sense that no superconductivity is detected for TiB_2 even below 1 K.⁵⁶

The role of Mg on the band structure of MgB_2 can be elucidated by completely removing the Mg atoms from the lattice and repeating the calculations for a hypothetical structure with only B atoms (note: using the lattice parameters for MgB_2). The calculated electronic structure for B network alone is given in Fig.2 along with that of MgB_2 . The striking difference between the two cases is in the position of the flat band in the Γ -A direction. This flat band feature for the B network alone is strongly two dimensional (viz. very little dispersion along Γ -A). This is ca. 1.8 eV above E_F owing to the lower number of electrons in the B network compared with MgB_2 . This suggests that the B-B σ bonds are primarily responsible for the superconductivity in MgB_2 . Interestingly the bands are not deformed appreciably when we remove Mg from MgB_2 indicating that the electrons from Mg atoms mainly give a shift in E_F almost like rigid-band filling. This view point is confirmed also from the density of states study (see Fig.,3) which shows that the topology of the DOS profile with and without Mg atoms in MgB_2 are almost the same. But a shift in DOS is observed when Mg is removed from MgB_2 .

BeB_2 could be expected to have a high T_c owing to the lighter Be atoms which may

provide larger phonon frequencies while maintaining a similar electronic structure to that of MgB₂. Even though BeB₂ is isoelectronic with MgB₂, the recent experimental study³⁶ did not reveal any sign of superconductivity down to 5 K. This negative finding makes it interesting to investigate the electronic structure of BeB₂ in detail. The lattice constants for BeB₂ obtained⁵⁷ by averaging experimental data for the actual unit cell have been inferred to be $a = 2.94$ and $c = 2.87$ Å. There are no experimental lattice parameters available for BeB₂ with the AlB₂-type structure and hence we have made structural optimization using the FPLAPW method. Table I shows that a is reduced only by about 1.6%, whereas c is by about 8% when Mg is replaced by Be. The anisotropic changes of the lattice parameters can be understood from the anisotropic bonding situation in MgB₂. It looks as if the strong B ($p-p$) σ bonds within the planes prevent more appreciable changes in a whereas the weaker π bonds along with the relatively weak ionic bonding between Be and B bring about a larger change in the c . Consistent with the earlier calculation⁵⁸ our calculated value of DOS at E_F for BeB₂ is smaller than that of MgB₂. The smaller $N(E_F)$ value results from the broad nature of band structure of BeB₂ compared with that of MgB₂. Owing to the smaller volume our calculated bulk modulus for BeB₂ becomes larger than that of MgB₂ (see Table I).

The total DOS curve for BeB₂ (see Fig. 4) shows almost free-electron-like metallic feature, with a $N(E_F)$ value of 6.309 state Ry⁻¹ f.u.⁻¹ which in turn is consistent with the paramagnetic behavior observed experimentally. The DOS curves of BeB₂ and MgB₂ are indeed very similar as expected due to their isoelectronic and postulated isostructural nature. As mentioned above the DOS features could lead one to a higher T_c for BeB₂ than for MgB₂ (the molecular weight of BeB₂ is lower than that of MgB₂). Hirish predicted⁵ that the charge transfer from Be to B in BeB₂ is less than that from Mg to B in MgB₂ and that E_F is below the regime where superconductivity occurs. A closer inspection of the band structure (see Fig. 5) indicates that the key energy band, which we believe to be responsible for superconductivity, is broader in BeB₂ than in MgB₂ and it is also located well above E_F . Hence the calculation suggests that even if one stabilizes BeB₂ in the AlB₂-type structure one can not expect superconductivity. Our conclusion is consistent with the experimental observation in the sense that a recent study³⁶ shows paramagnetic behavior down to 5 K.

Kortus *et al.*⁴ suggested that Ca doping should lead to an overall increase in DOS, and also provide an additional contribution to the electron-phonon coupling. We have therefore calculated DOS (using the optimized structural parameters) for CaB₂ which shows (Fig. 4) sharp features like those found in transition metal phases resulting from enhancement in volume compared with MgB₂. Also, the calculated DOS at E_F is larger than that of MgB₂ indicating a possibility for superconductivity. The larger volume compared with BeB₂ and MgB₂ along with the weak B-B interaction make the bulk modulus for this material become smaller. The electronic structure of CaB₂ (Fig. 5) shows that the key energy band is broader than that in MgB₂. Also this doubly degenerate band is well below E_F at the Γ point and well above E_F at the A point. Hence, the calculations suggest that the probability for superconductivity in CaB₂ with AlB₂-type structure is low.

The total DOS for SrB₂ (see Fig. 4) predicts a pseudogap feature at E_F (separating bonding from antibonding states with a negligible DOS at E_F). The electronic structure of SrB₂ (Fig. 5) shows nearly semimetallic feature. Earlier studies^{59,55} indicate that materials with E_F located at a pseudogap in DOS will have relatively high stability. (The situation

with all bonding orbitals filled and all antibonding orbitals empty implies extra contribution to stability.) Hence the calculations predict that SrB₂ with AlB₂ structure may be stabilized experimentally if the above criterion works. However, materials with E_F located in the pseudogap are not expected to become superconducting⁵⁴ and hence the present finding suggests that SrB₂ should be non-superconducting. Compared to BeB₂ and MgB₂, the top of the VB in CaB₂ and SrB₂ have large nonbonding B p states (see Fig. 4). This will give negative contribution to the one-electron eigen-value sum for stability. This may be the reason why no stable CaB₂ and SrB₂ compounds are stabilised experimentally in the AlB₂ structure.

The number of valence electrons per B, C atom is same for LiBC and MgB₂. So, if electron per atom ratio is the decisive factor for the superconducting behavior of MgB₂ one can expect superconductivity for LiBC. Hence, we have also performed electronic structure studies for LiBC. The calculated DOS (Fig. 4) predicts insulating behavior with a band gap of 1.81 eV. LiBC is an indirect bandgap insulator where the bandgap is between the top of VB in the Γ -K direction and the bottom of CB at the M point (Fig. 6). The establishment of insulating behavior is consistent with the experimental observation⁶⁰ of a very small conductivity for LiBC. The flat band feature present in the K-M and Γ -A directions of the BZ just below E_F around -0.23 eV (see Fig. 6) suggests that LiBC may be tuned to become superconducting upon hole doping.

The calculated total DOS (Fig. 4) for MgB₂C₂ shows a finite number of electrons at E_F (which has the same number of valence electrons per non-metal atom as MgB₂) and predicts metallic behavior. This is further confirmed by the band structure (Fig. 6) which shows that several bands cross the Fermi level. The most interesting aspect of Fig. 6 is that there is flat band present in the vicinity of E_F (around the T-Y direction) similar to that in MgB₂ and superconducting transition metal borocarbides (e.g, YNi₂B₂C, LuNi₂B₂C). Consequently we suggest superconductivity with relatively high T_c for MgB₂C₂. A more detailed analysis of the band structure shows that the narrow band in the T-Y direction near E_F is stemming from the C p_z electrons. The calculated density of states at E_F for MgB₂C₂ is 10.98 states Ry⁻¹ f.u.⁻¹ which is higher than for MgB₂. Except for the structural data⁶¹ no other information on the physical properties of MgB₂C₂ are available experimentally which may be a promising candidate for high T_c superconductivity.

If it is the boron layers that are responsible for the superconductivity, one could expect superconductivity in MgB₄. However, the calculated total DOS for MgB₄ shows (Fig. 4) only features which point towards insulating behavior and hence superconductivity is not expected for this material.

B. Superconductivity

Let us first look for similarities between MgB₂ and other superconducting materials. There appears to be different correlations⁶² between superconducting transition temperature and the average electronegativity (η) for high T_c cuprates and conventional superconductors. Conventional superconductors take η value between 1.3 and 1.9 whereas that for high T_c cuprates falls in the range 2.43 to 2.68.⁶³ The η value for MgB₂ is 1.733 which places this material in the category of the conventional superconductors. However, using the proposed correlation⁶⁴ between superconducting transition temperature and the value of electronic

specific heat coefficient (γ) for various superconductors we find that γ for MgB₂ falls in the region of the high T_c cuprates (viz. MgB₂ has a low value of $N(E_F)$ as well as high T_c). In the conventional superconductors (A15-type) with A₃B composition, the mutually orthogonally permuted linear ..A-A-A.. chains are believed to be responsible for the superconductivity. In MgB₂, the B atoms in the zig-zag chains are believed to be playing an important role for superconducting behavior. For higher T_c of superconducting intermetallics Butler⁶⁵ has suggested a rule of togetherness which prescribes that (for a given crystal structure, electron-per-atom ratio and period) the electron-phonon coupling is enhanced when the transition metal atoms are brought closer together. It is interesting to note that the B atoms are brought close together by the strong covalent bonding in MgB₂. Earlier studies⁶⁶ show that β -ZrNCl is a semiconductor with a band gap of ~ 3 eV that upon Li intercalation (the electron donor element) becomes superconducting with $T_c = 13$ K.²⁸ This similarity is present for MgB₂ also, that the electron donation from Mg to B₂ leads to superconductivity. Ledbetter⁶⁷ points out that the superconducting transition temperature in high T_c cuprates increases with increasing Debye temperature (θ_D). The high T_c in MgB₂ may be associated with the large θ_D in this material and this criterion would place MgB₂ with high T_c cuprates.

In conventional superconductors, T_c increases with decreasing θ_D , i.e. with lattice softening.⁶⁷ The calculated θ_D for MgB₂ from the elastic constants is 1016 K which is found to be much higher value than in phonon mediated superconducting materials. However, the calculated value of θ_D is comparable with the experimental values obtained from specific heat measurements (Table II). The presently derived θ_D is exceptionally large indicating that some novel mechanism is responsible for the high T_c in MgB₂. Concerning the relationship of the purely phononic properties to superconductivity, owing to the large θ_D , average phonon properties cannot reliably be used to estimate superconducting properties for this material. Using the concept that temperature-dependent electronic screening arising from narrow bands in the vicinity of E_F causes temperature-dependent phonon-mode frequencies (see Fig. 2), one is lead to expect that softening of phonon modes does occur. Therefore, experimental temperature dependent phonon spectra for MgB₂ is required to establish whether softening of particular phonon modes is responsible for its large T_c .

The BCS theory and its subsequent refinements based on Eliashberg equations show that high T_c in phonon-mediated superconductors is favored by high phonon frequency and a large DOS at E_F . High T_c materials commonly display interesting peculiarities in the phonon-dispersion curves, often in the form of dips (i.e. softening of phonons in well-defined regions of reciprocal space) which are particularly evident when phonon spectrum of a high- T_c material is compared with that of a similar low- T_c material (such as Nb vs. Mo, TaC vs. HfC). Assuming that this is the case for MgB₂ the high T_c can be explained as follows. The superconducting transition temperature for the strongly coupled superconductors according to the McMillan's formula⁶⁸ is,

$$T_c = \frac{\theta_D}{1.45} \exp\left[-\frac{1.04(1 + \lambda)}{\lambda - \mu^*(1 + 0.62\lambda)}\right] \quad (3)$$

In Eqn. III B large T_c can be obtained when we have a large value for θ_D (which MgB₂ has) and the electron-phonon coupling constant λ . The empirical value of the Coulomb coupling constant μ^* for *sp* metals is 0.1. The McMillan-Hopfield expression for $\lambda = \frac{N(E_F)\langle I^2 \rangle}{M\langle \omega^2 \rangle}$, which enters in the exponent in the expression for T_c . Here, $N(E_F)$ is smaller for MgB₂ than for

conventional high T_c materials, $\langle I^2 \rangle$ is the averaged square of the electron-phonon matrix element, $\langle \omega^2 \rangle$ is the averaged square of the phonon frequency and M is the mass of the ion involved. If the superconductivity occurs by phonon mediation, high T_c in MgB₂ can be explained as follows. Selected phonon modes may be strongly coupled to the electronic system and influence the magnitude of T_c to a greater extent than average phonon modes. In consistent with the above view point the lattice dynamical calculations^{21,69,70,7} reveal that the in-plane boron phonons near the zone-center are highly anharmonic with significant non-linear contribution to the electron-phonon coupling. If such a situation occurs, the softening of certain phonons in combination with the light mass of the constituents may lower the phonon contribution ($M < \omega_{ph}^2$) and in turn enhance the electron-phonon coupling constant and hence T_c . This may explain why MgB₂ possesses high T_c despite the lower value of $N(E_F)$.

Now we will compare MgB₂ with relevant superconducting material. Among the other transition metal diborides, superconductivity with $T_c=9.5$ K has been observed in TaB₂ recently.⁷¹ Our electronic structure studies⁵⁵ show that the E_F is located in a peak in the DOS profile in TaB₂. This feature along with the large $N(E_F)$ value of 12.92 states/(Ry f.u.) will explain the large T_c in this material. As there is substantial B p states present at E_F in MgB₂ similar to superconducting RNi₂B₂C, it may be worthwhile to compare these two cases. An experimental soft x-ray emission spectroscopy study⁷² on superconducting YNi₂B₂C and non-superconducting LaNi₂B₂C along with bandstructure calculation⁷³ indicate that the superconductivity appears only when the broad B p bands are located at E_F . The main difference between the electrons involved in transport properties of RNi₂B₂C and MgB₂ is that the former has a remarkable DOS peak at E_F dominated by Ni 3d states with almost equal proportions of all five Ni 3d states and also involves some rare-earth d and B, C sp admixture whereas MgB₂ does not show any peak feature at E_F . From the accurate analysis of measured⁷⁴ specific heat over a wide temperature range the estimated γ for MgB₂ is estimated as 5.5 mJ/mol K². From our calculated $N(E_F)$ value we have derived the electronic contribution to the specific-heat coefficient without electron-phonon mass enhancement yield a value of 1.73 mJ/mol K². From this value along with the experimental γ_{exp} we have estimated the value of electron-phonon coupling constant using the relation $\gamma_{exp} = \gamma_{th}(1 + \lambda)$ which gave $\lambda = 2.17$. The large λ value indicates MgB₂ is a strongly coupled superconductor. This strong coupling as well as the low mass of B can explain the high T_c in MgB₂.

Using the calculated plasma frequency (Ω_{px}) in the ab plane (7.13 eV) along with $N(E_F) = 0.71$ states/(eV f.u.) the in-plane Fermi velocity ν_{Fx} has been obtained as

$$\nu_{Fx} = \sqrt{\frac{\Omega_{px}^2}{4\pi e^2 N(E_F)}} = 8.9 \times 10^7 \text{ cm/s}.$$

Using the superconducting gap $\Delta=3.53k_B T_c/2 = 6$ meV we have calculated the coherence length (ξ) and the field penetration depth (Λ)

$$\xi = \frac{\hbar \nu_{Fx}}{\pi \Delta} = 307 \text{ \AA}; \Lambda = \frac{c}{\Omega_{px}} = 276 \text{ \AA}.$$

The experimental upper critical field, $H_{c2}(T)$, thermodynamic critical field, $H_c(T)$, and critical current, J_c , indicate that MgB₂ is a type-II superconductor.⁷⁵

Now we will try to understand the effect of pressure on the superconductivity in MgB₂. Addition of Mg to the boron sublattice gives 15% shortening of the c axis compared to that in graphite.¹¹ This chemical pressure brings the B semimetal to superconducting state. As the transport properties of MgB₂ is from the holes, it is suggested that the superconductivity may be understood within the formalism developed for high- T_c cuprate superconductors.⁵ This predicts a positive pressure coefficient for T_c as a result of the decreasing intraplane B-B distance with increasing pressure. However, the T_c is experimentally³¹ found to decrease with pressure at a rate of -1.11 K/GPa. The RVB theory,¹¹ on the other hand, predicts a decrease in T_c with increasing chemical pressure, consistent with the experimental findings.^{31,76,77} Linear response calculations²¹ show that the B-bond stretching modes have unusually strong coupling to electrons close to E_F at the top of the bonding quasi-two-dimensional B σ bonds. Therefore, when the compressibility is larger within the ab plane than along c , one can expect a large variation in the superconductivity with pressure (because the flat bands with $p_{x,y}$ characters broaden faster by compression). Our calculated elastic property for MgB₂ shows large anisotropy with easy compression along c . Hence, the key energy band (which is sensitive to the B bond stretching) will broaden slowly with pressure and T_c will slowly decrease with increasing pressure, consistent with experimental results.

From the FPLAPW calculations we have estimated the electric field gradient (V_{zz}) at the Mg and B site as -0.249×10^{21} and 2.047×10^{21} V/m², respectively. Using the calculated V_{zz} along with the nuclear quadrupole moment for ¹¹B (0.037 b)⁷⁸ we can calculate the NMR quadrupole coupling frequency (ν_q) by means of the relation

$$\nu_q = \frac{3eQV_{zz}}{2hI(2I - 1)}$$

using $I = 3/2$ as the nuclear spin quantum number for ¹¹B. This gave $\nu_q = 915$ kHz that is in good agreement with 828 kHz obtained by Gerashenko *et al.*¹³ and 835 ± 5 kHz obtained by Jung *et al.* from first order quadrupole perturbed NMR spectrum.¹⁴

C. Chemical bonding in MgB₂

Similar to the C-C distances in the graphite structure, the distance between the boron planes in MgB₂ is about twice the intraplanar B-B distance and hence the B-B bonding is strongly anisotropic. A more quantitative assessment of the bonding situation in MgB₂ can be obtained from the partial DOS (Fig.3) which demonstrates that the B s states are hybridized with the B p state in VB. This shows strongly bonded sp^2 hybrids in the ab plane. The Mg s electrons contribute very little to the VB and are mainly reflected in the unoccupied state. Hence Mg donates electrons to the boron layers. VB carries predominantly B $2p$ character formed from two distinct sets [σ ($p_{x,y}$) and π (p_z)] of bonds. The B $2s$ electrons are well localized and their contribution at E_F is minor. From the orbital projected DOS (Fig. 3) it is clear that B p_x and p_y characters are mainly dominating at E_F . This suggests that the $p - p$ σ bonding between the boron atoms has a significant influence on superconductivity. It is worth to recall that the recently found²⁸ superconductor Na_{0.29}HfNCl ($T_c \approx 25$ K) has N p_x and p_y characters at E_F .⁷⁹ B p_z states are present in a wide energy range and dominating at the bottom of CB.

The simplest way to investigate the bonding situation between two interacting atoms in solid is to inspect the complete COHP between them, taking all valence orbitals into account. In the upper panel of Fig 3 shows COHP for the B-B and Mg-B bonds. An interesting aspect of this illustration is that VB is filled up with bonding orbitals (negative value of COHP) and the antibonding orbitals are some ~ 3 eV above E_F . Bonding state electrons from both B-B and Mg-B bonds are found at E_F . The B $s - s$ bonding states are found mainly at the bottom of VB around -8.5 eV. The B $p - p \sigma$ bonding states dominate at the top of the VB region around -2 eV. Note that the COHP values for the Mg-B bonds are much smaller than for the B-B bonds indicating that the B-B bond is much stronger than the Mg-B bonds. In order to quantify the bonding interactions in MgB_2 we have integrated the COHP curve and obtained the values -4.36 , -1.23 and -0.307 eV for B-B, Mg-B and Mg-Mg bonds respectively. This further confirms that the B-B bonds are the strongest in MgB_2 which in turn consistent with the derived elastic properties (see Sec. III D).

In order to further illustrate the bonding situation in MgB_2 a charge density plot for the (110) plane is shown in Fig. 7. This illustration shows a low electron accumulation between Mg and B as well as a very low electron population at the Mg site (much lower than for a neutral Mg atom). These findings are a clear indication of ionic bonding between Mg and B. The large electron accumulation between the B atoms and their strongly aspherical character indicate strong covalent interaction between the B atoms as also found by our examination of partial DOS and COHP. The more or less homogeneous charge distribution between the Mg atoms suggest an appreciable degree of metallic bonding between them. i.e. apart from strong ionic and covalent bonding in MgB_2 the band structure shows features similar to the sp metals. Hence, MgB_2 is a typical example of a mixed bonded solid.

D. Elastic properties

Structural parameters for BeB_2 , CaB_2 , SrB_2 are not available experimentally and we have therefore made structural optimization for these diborides along with the MgB_2 by total energy minimization. The calculated total energy variation as a function of c/a and volume for MgB_2 is shown in Fig. 8a and 8b respectively. The optimized structural parameters along with the bulk modulus, its pressure derivative and DOS at E_F for all these diborides are given in Table I. The calculated equilibrium volume for MgB_2 is found to be in excellent agreement with the experimental value,⁴⁰ and the corresponding c/a value is only 0.42% smaller than the experimental value (see Fig. 8b and Table I). These results indicate that density functional theory works well for this material. The calculated $N(E_F)$ value for MgB_2 is larger than that for other diborides considered in the present study and this may be one of the reasons for the superconductivity in MgB_2 .

By fitting the total-energy vs. volume curve in Fig. 8 to the universal equation of state we have obtained the bulk modulus (B_0) and its pressure derivative (B'_0) as 1.50 Mbar and 3.47, respectively. The derived B_0 is found to be in excellent agreement with the value 1.51 Mbar obtained from high resolution x-ray powder diffraction measurements³³ and also in good agreement with other results listed in Table I. Furthermore $B_0 = 1.5$ Mbar obtained in this way is in good agreement with the value 1.509 Mbar estimated from the calculated single-crystal elastic constants by means of the relation

$$B = \frac{2(c_{11} + c_{12}) + 4c_{13} + c_{33}}{9}.$$

The electron per atom ratio of TiB₂ is same as that of MgB₂ and hence this material should also be considered. In TiB₂ E_F is located in a pseudogap and hence $N(E_F)$ is small resulting in non-observation of superconductivity. The calculated bulk modulus for TiB₂ is larger than that for diborides considered in the present study. This is an effect of the filling of the bonding states in the bands and this aspect has been discussed in Ref. 55.

From various distortions we have calculated all the five single-crystal elastic constants for MgB₂ (see Table III). Unfortunately there are no experimental elastic constants available since a suitable single crystal of MgB₂ has so far not been obtained. We have therefore made comparison with the data for TiB₂ available experimentally⁸⁰. Despite the layered crystal structure of MgB₂ the high pressure total energy studies of Loa and Syassen³² suggested isotropic compressibility and they concluded that the intra- and the interlayer bonding are of similar strength. Another high pressure study (upto 8 Gpa) by Vogt *et al.*³³ concluded that there are small anisotropies in the mechanical properties. The isothermal compressibility measurements of MgB₂ by synchrotron x-ray diffraction revealed³⁴ a stiff tightly-packed incompressible nature with only moderate anisotropy between intra- and interlayer bonds. The neutron diffraction measurements by Jorgensen *et al.*³⁵ at high pressures concluded with highly anisotropic mechanical properties for MgB₂. As the experimental results are mutually inconsistent, theoretical studies of the compressibility may be helpful in resolving the ambiguities.

From the calculated single-crystal elastic constants we have derived the bulk moduli along the crystallographic directions using the relations given in Sec. II and the results are listed in Table III. The compressibility study³⁴ by synchrotron radiation show isothermal interlayer compressibility, $dlnc/dP$ at zero pressure is 1.4 times the inplane compressibility, $dlna/dP$. However the high pressure neutron diffraction studies³⁵ show that $dlnc/dP=1.64 dlna/dP$ which is much closer to our calculated relationship $dlnc/dP=1.79 dlna/dP$ (see Table III). The most recent high pressure measurement⁸¹ by hydrostatic pressure upto 15 GPa shows a large anisotropy with the relationship $dlnc/dP=1.875 dlna/dP$. The higher compressibility along c than along a can be understood as follows. There is strong B $p_{x,y} - p_{x,y}$ covalent hybridization along a in MgB₂ and hence the bulk modulus along a (b) is large. There is significant ionic contribution to the bonding between Mg and B along c . Usually an ionic bond is weaker than a covalent bond and hence the bulk modulus is smaller along c than along a . The large anisotropy in the compressibility is also consistent with the fact³⁵ that the thermal expansion of c is about twice as that of a . Moreover, substitution¹⁶ of Al for Mg site decreases c at a rate approximately twice that of a indicating the anisotropic nature of bonding.

It is possible to visualize the anisotropy in the elastic properties from the curvature of the total energy with respect to length changes in an arbitrary direction. From the elastic compliance constants (s_{ij}) it is possible to derive the directional bulk modulus K , using the following relation:⁸²

$$\frac{1}{K} = (s_{11} + s_{12} + s_{13}) - (s_{11} + s_{12} - s_{13} - s_{33})l_3^2 \quad (4)$$

where l_3 is the direction cosine. Thus obtained directional dependent bulk modulus is shown

in Fig. 9a. A useful surface construction is one that shows the directional dependence of Young's modulus (E), which for hexagonal symmetry can be defined as

$$\frac{1}{E} = (1 - l_3^2)^2 s_{11} + l_3^4 s_{33} + l_3^2 (1 - l_3^2) (2s_{13} + s_{44}) \quad (5)$$

Thus derived directional-dependent Young's modulus (Fig. 9b) also shows large anisotropy, E along a being about 65% larger than along c . The anisotropic nature of bonding behavior reflected in the elastic properties is consistent with the charge density analysis. The marked anisotropic compressibility of MgB₂ will lead to different pressure effects on different phonon modes and is also more likely to lead to pressure induced changes in the electronic structure at E_F . This information is valuable in testing the predictions of competing models^{5,11} for the mechanism of superconductivity.

The anisotropy in the plastic properties of materials can be studied from the directional dependent shear stress and the amount of shear.⁸³ So, it is interesting to study the directional dependence of shear in MgB₂. We have calculated the directional dependent shear modulus (G) from the elastic constants using the relation

$$\frac{1}{G} = s_{44} + (s_{11} - s_{12} - \frac{s_{44}}{2})(1 - l_3^2) + 2(s_{11} + s_{33} - 2s_{13} - s_{44})(1 - l_3^2)l_3^2 \quad (6)$$

The directional dependent shear modulus (see Fig. 9c) also shows large anisotropy and the G along the a axis is around 42% higher than that along c . It should be noted that large shear value is present in between the basal plane and perpendicular to basal plane. From the calculated directional dependent bulk modulus and the shear modulus one can calculate the directional dependence of sound velocity and hence the characteristic temperature of the material. The calculated characteristic temperature given in Fig. 9d shows anisotropic nature due to the anisotropy in the bonding behavior. The calculated average shear modulus (G_{av}), elastic-wave velocities (ν) and θ_D obtained from our single crystal elastic constants are listed in Table II. The calculated θ_D for MgB₂ is much higher than the experimental values and the higher value of θ_D indicates that higher phonon frequencies play an important role for the high T_c of this material. The existence of phonon modes at very high energies as 97 meV in MgB₂ is experimentally identified by neutron-inelastic-scattering measurements.^{15,84} One of the reasons for the discrepancy between the θ_D obtained from the elastic constants and the specific heat measurements is as follows. For example, the experimental electrical resistivity and specific heat measurements on TiSi₂ gave $\theta_D = 560$ - 664 K, whereas elastic constants measurements gave $\theta_D = 700$ K (that is in close agreement with $\theta_D = 722$ K obtained from our theoretical elastic constant calculations⁸⁵). So, one can expect good agreement when comparing our θ_D with that obtained from elastic constants measurement.

E. Optical properties

Optical properties studies are of fundamental importance, since these involve not only the occupied and unoccupied parts of the electronic structure but also carries information on the character of the bands. In order to elucidate the anisotropy in the optical properties of MgB₂ the calculated imaginary parts of dielectric tensor for $E||a$ and $E||c$ are shown in Fig. 10. The important feature conveyed by the interband transition shown in Fig.10 is that there is

negligible contribution to $\epsilon_2(\omega)$ in $E\parallel c$ below 3.8 eV. The interesting aspect for MgB₂ is that even though the interband contribution to the optical spectra is highly anisotropic the calculated intraband contribution show nearly isotropic behavior. This originates from the close values of the calculated plasma frequencies; 7.13 and 6.72 eV for in-plane and perpendicular to the plane, respectively. These values are in excellent agreement with $\omega_{p,x} = 7.02$ eV and $\omega_{p,z} = 6.68$ eV obtained by full-potential LMTO calculation.²¹ The intraband contribution to the optical dielectric tensor have been calculated similar to our earlier study.⁵² The calculated $\epsilon_2(\omega)$ spectra which include both inter- and intraband contributions are shown in the upper panel of fig.10. From these $\epsilon_2(\omega)$ spectra one can derive all linear optical properties. Unfortunately, there are no experimental spectra available for MgB₂.

IV. SUMMARY

The present study shows a common origin between the superconductivity in rare earth transition metal borocarbides and MgB₂ that there is a flat band present in the vicinity of Fermi level and also the B atoms are primarily involved in electron-phonon coupling in these materials. Owing to the lack of single crystals the anisotropy in physical properties of MgB₂ are not studied experimentally. We predicted large anisotropies in the optical and mechanical properties. From detailed electronic structure studies we have arrived at the following conclusions.

1. The bonding behavior in MgB₂ has been explained by analyses of site, angular momentum and orbital projected density of states as well as charge density and crystal overlap Hamiltonian population. These analyses establish a mixed bonding behavior with ionic bonding between Mg and B, covalent bonding between B atoms and metallic bonding between Mg and Mg like that in *sp* metals.
2. We identified a large anisotropy in the mechanical properties of MgB₂ from our calculated elastic constants, consistent with the anisotropy in the bonding behavior and high pressure neutron diffraction measurements. Consequently, pressure can influence the bands in different directions of the BZ in an unusually different manner and hence the physical properties.
3. Two degenerate flat bands have been identified near E_F in the Γ -A direction of BZ. These degenerate B $p_{x,y}$ bands are considered as the key in the realization of the high temperature superconductivity of MgB₂.
4. The role of Mg in MgB₂ is to donate electrons to B atoms and hence to shift E_F such that it lies very closer to the flat band, the feature which we believe important for superconductivity.
5. We found similarity in the electronic structures of MgB₂ LiBC and MgB₂C₂. Therefore superconductivity is expected in MgB₂C₂ and hole doped LiBC. On the other hand the electronic structure of BeB₂, CaB₂, SrB₂ and MgB₄ suggest a low probability for superconductivity.

6. Because of the nearly flat bands in the vicinity of E_F (which will introduce temperature depending electronic screening of the phonon-mode frequencies), we expect temperature-dependent phonon-mode softening or large anisotropy in the phonon modes.
7. The calculated boron NMR frequency is found to be in very good agreement with the experimental studies.
8. As our calculated Debye temperature for MgB_2 is much larger than for other superconducting intermetallics, we believe that selected phonon modes can be strongly coupled to the electronic system and thus influence the magnitude of T_c to a greater extent than the average phonon correlations may indicate.
9. If the rigid band-filling approximation works and also the electrons are responsible for superconductivity in MgB_2 , our calculation suggests that a doping of 0.32 electrons will enhance T_c . However, the experimental observation of reduction in T_c by electron doping in MgB_2 indicate that the holes are responsible for superconductivity.

ACKNOWLEDGMENTS

PR is grateful for the financial support from the Research Council of Norway. Part of these calculations were carried out on the Norwegian supercomputer facilities (Programme for Supercomputing). PR wishes to acknowledge Prof.O.K.Andersen, Prof.Ove Jepsen, Dr.Florent Boucher, Dr.John Wills, Prof.K.Schwarz and Prof.Peter Blaha for providing some of the programmes used in this study, and Dr.Anna Delin and Dr.Lars Fast for useful communications.

REFERENCES

- * Electronic address: ravindran.ponniah@kjemi.uio.no
- ¹ J.Nagamatsu, N.Nakagawa, T.Muranaka, Y.Zenitani and J.Akimitsu, *Nature* **410**, 63 (2001).
 - ² J.G.Bednorz, K.A.Müller, *Z. Phys. B*, **64**, 189 (1986).
 - ³ L.Gao, Y.Y.Xue, F.Chen, Q. Ziong, R.L. Mentg, D.Ramirez, C.W.Chu, J.H.Eggert, H.K.Mao, *Phys. Rev. B*, **50**, 4260 (1994).
 - ⁴ J.Kortus, I.I.Mazin, K.D.Belashchenko, A.P.Antropov and L.L.Boyer, Preprint cond-mat/0101446 (2001).
 - ⁵ J.E.Hirsch, Preprint, cond-mat/0102115 (2001).
 - ⁶ K.D. Belashchenko, M. van Schilfgaarde and V.P.Antropov, Preprint, cond-mat/0102290 (2001).
 - ⁷ J.M.An and W.E.Pickett, Preprint, cond-mat/0102391 (2001)
 - ⁸ W.N.Kang, C.U.Jung, K.H.P.Kim, M.S.Park, S.Y.Lee, H.J.Kim, E.M.Choi, K.H.Kim, M.S.Kim and S.L.Lee, Preprint, cond-mat/0102313 (2001).
 - ⁹ A.K.Gangopadhyay, A.J.Schwetz and J.S.Schilling, *Physica C*, **246**, 317 (1995).
 - ¹⁰ S.L.Bud'ko, G.Lapertot, C.Petrovic, C.E.Cunningham, N.Anderson and P.C.Canfield, *Phys. Rev. Lett.*, **86**, 1877 (2001).
 - ¹¹ G.Baskaran, Preprint, cond-mat/0103308 (2001).
 - ¹² H.Kotegawa, K.Ishida, Y.Kitaoka, T.Muranaka and J.Akimitsu, Preprint, cond-mat/0102334 (2001).
 - ¹³ A.Gerashenko, K.Mikhalev, S.Verkhovskii, T. D'yachkova, A.Tyntynnik, V.Zubkov, Preprint, cond-mat/0102421 (2001).
 - ¹⁴ J.K.Jung, S.H.Baek, F.Borsa, S.L.Bud'ko, G.Lapertot and P.C.Canfield, Preprint, cond-mat/0103040 (2001).
 - ¹⁵ T.J.Sato, K. Shibata and Y.Takano, Preprint, cond-mat/0102468 (2001).
 - ¹⁶ J.S.Slusky, N.Rogado, K.A.Regan, M.A.Hayward, P.Khalifah, T.He, K.Inumaru, S.Loureiro, M.K.Haas, H.W.Zandbergen and R.J.Cava, Preprint, cond-mat/0102262 (2001).
 - ¹⁷ J.S.Ahn and E.J.Choi, Preprint, cond-mat/0103169 (2001)
 - ¹⁸ T. Takenobu, T.Ito, D.H. Chi, K. Prassides and Y. Iwasa, Preprint, cond-mat/0103241 (2001).
 - ¹⁹ W.N. Kang, C.U. Jung, K.H.P. Kim, M.S. Park, S.Y. Lee, H.J. Kim, E.M. Choi, K.H. Kim, M.S. Kim, S.I. Lee, Preprint, cond-mat/0102313 (2001).
 - ²⁰ C. Panagopoulos, B.D. Rainford, T.Xiang, C.A.Scott, M.Kambara, I.H.Inoue, Preprint, cond-mat/0103060 (2001)
 - ²¹ Y.Kong, O.V.Dolgov, O.Jepsen and O.K.Andersen, Preprint, cond-mat/0102499 (2001).
 - ²² R.Nagarajan, C.Mazumdar, Z.Hossain, S.K.Dhar, K.V.Gopalakrishnan, L.C.Gupta, C.Godart, B.D.Padalia and R.Vijayaraghavan, *Phys. Rev. Lett.*, **72**, 274 (1994).
 - ²³ R.J.Cava, K.Takaki, B.Batlogg, H.W.Zandbergen, J.J.Krajewski, W.F.Peck Jr., R.B.van Dover, R.J.Felder, T.Siegrist, K.Mizuhahi, J.O.Lee, H.Elsaki, S.A.Carter and S.Uchida, *Nature*, **367**, 146 (1994); R.J.Cava, H.Takagi, H.W.Zandbergen, J.J.Krajewski, W.F.Peck Jr., T.Siegrist, B.Batlogg, R.B. van Dover, R.J.Felder, K.Mizuhashi, J.O.Lee, H.Eisaki and S.Uchida, *Nature*, **367**, 252 (1994).
 - ²⁴ R.J.Cava, H.W.Zandbergen, B.Batlogg, H.Eisaki, H.Tagaki, J.J.Krajewski, W.F.Peck

- Jr., E.M. Gyorgy and S. Uchida, *Nature*, **372**, 245 (1994); H.W. Zandbergen, J. Jansen, R.J. Cava, J.J. Krajewski, W.F. Peck Jr., *Nature*, **372**, 759 (1994).
- ²⁵ A.D. Chinchure, R. Nagarajan and L.C. Gupta, *Physica B*, **281 & 282**, 894 (2000).
- ²⁶ J.C. Philips, *Physics of High T_c Superconductors*, Academic Press, New York (1989).
- ²⁷ K.P. Sinha and S.L. Kakani, *Magnetic Superconductors*, Nova Science, Commack, (1989).
- ²⁸ S. Yamanaka, H. Kawaji, K. Hotehama and M. Ohashi, *Adv. Mater.* **9**, 771 (1996); S. Yamanaka, K. Hotehama, and H. Kawaji, *Nature (London)*, **392**, 580 (1998).
- ²⁹ R.K. Kremer, K. Ahn, R.W. Henn, J.J. Mattausch, W. Schndle, A. Stolovits, and A. Simon, *Physica C*, **317 & 318**, 456 (1999).
- ³⁰ S. Sanfilippo *et al.*, *Phys. Rev. B* **61**, R3800 (2000).
- ³¹ T. Tomita, J.J. Hamlin, J.S. Shilling, D.G. Hinks and J.D. Jorgensen, Preprint, cond-mat/0103538 (2001).
- ³² I. Loa and K. Syassen, *Solid State Commun.* in press (2001).
- ³³ T. Vogt, G. Schneider, J.A. Hriljac, G. Yang and J.S. Abell, Preprint, cond-mat/0102480 (2001).
- ³⁴ K. Prassides, Y. Iwasa, T. Ito, D.H. Chi, K. Uehara, E. Nishibori, M. Takata, S. Sakata, Y. Ohishi, O. Shimomura, T. Muranaka and J. Akimitsus, Preprint, cond-mat/0102507 (2001).
- ³⁵ J.D. Jorgensen, D.G. Hinks and S. Short, Preprint, cond-mat/0103069 (2001).
- ³⁶ I. Felner, Preprint, Preprint, cond-mat/0102508 (2001).
- ³⁷ S.M. Kazakov, M. Angst and J. Karpinski, Preprint, cond-mat/0103350 (2001).
- ³⁸ Y.G. Zhao, X.P. Zhang, P.T. Qiao, H.T. Zhang, S.L. Jia, B.S. Cao, M.H. Zhu, Z.H. Han, X.L. Wang and B.L. Gu, Preprint, cond-mat/0103077 (2001).
- ³⁹ N.I. Medvedeva, A.L. Ivanovskii, J.E. Medvedeva and A.J. Freeman, Preprint, cond-mat/0103157 (2001).
- ⁴⁰ M.E. Jones and R.E. Marsh, *J. Am. Chem. Soc.* **76**, 1434 (1954).
- ⁴¹ M. Wörle and R. Nesper, *J. Alloy. Compd.* **216**, 75 (1994)
- ⁴² M. Wörle and R. Nesper, *Z. Anorg. Allg. Chem.*, **621**, 1153
- ⁴³ A. Vegas, L.A. Martinez-Cruz, A. Ramos-Gallardo and A. Romero, *Z. Kristallogr.*, **210**, 575 (1995).
- ⁴⁴ P. Blaha, K. Schwarz and J. Luitz, WIEN97, Vienna University of Technology, 1997 (Improved and updated Unix version of the original copyrighted WIEN code, which was published by P. Blaha, K. Schwarz, P. Sorantin and S.B. Trickey, *Comput. Phys. Commun.*, **59** 399 (1990).
- ⁴⁵ J.P. Perdew, S. Burke and M. Ernzerhof, *Phys. Rev. Lett.*, **77**, 3865 (1996).
- ⁴⁶ O.K. Andersen and O. Jepsen, *Phys. Rev. Lett.*, **53**, 2571 (1984).
- ⁴⁷ R. Dronskowski, P.E. Blochl, *J. Phys. Chem.* **92**, 5397 (1993).
- ⁴⁸ G. Krier, O. Jepsen, A. Burkhardt, and O.K. Andersen, *Tight binding LMTO-ASA Program Version 4.7*, Stuttgart, Germany.
- ⁴⁹ J.M. Wills, O. Eriksson, M. Alouani and D.L. Price in *Electronic structure and Physical Properties of Solids*, P.148, Ed. H. Dreysse, Springer, Berlin (2000) ; J.M. Wills and B.R. Cooper, *Phys. Rev. B*, **36**, 3809 (1987); D.L. Price and B.R. Cooper, *Phys. Rev. B*, **39**, 4945 (1989).
- ⁵⁰ O.K. Andersen, *Phys. Rev. B*, **12**, 3060 (1975).
- ⁵¹ M. Alouani and J.M. Wills, *Phys. Rev. B*, **54**, 2480 (1996); R. Ahuja, S. Auluck, J.M. Wills,

- M.Alouani, B.Johansson and O.Eriksson, Phys. Rev. B, **55**, 4999 (1997).
- ⁵² P.Ravindran, A.Delin, B.Johansson, O.Eriksson and J.M.Wills, Phys. Rev. B, **59**, 1176 (1999).
- ⁵³ D.C.Wallace, Thermodynamics of Crystals, John Wiley & Sons, Newyork (1972).
- ⁵⁴ P. Ravindran and R. Asokamani, J. Phys. Condens. Matter, **7**, 1 (1995).
- ⁵⁵ P. Vajeeston, P. Ravindran, C. Ravi and R. Asokamani, Phys. Rev. B, **63**, 045115 (2001).
- ⁵⁶ L.Leyarovska and E.Leyarovski, J. Less-Common Met. **67**, 249 (1979).
- ⁵⁷ I.I.Tupitsyn et al., Sov. Phys. Solid State **16**, 2015 (1975).
- ⁵⁸ G.Satta, G.Profeta, F.Bernardini, A.Continenza and S.Massidda, Preprint, cond-mat/0102358 (2001).
- ⁵⁹ P.Ravindran, G.Subramonium and R.Asokamani, Physical Rev. B, **53**, 1129 (1996).
- ⁶⁰ M.Wörle, R.Nesper, G.Mair, M.Schwarz and H.G.von Schnering, Z. Anorg. Allg. Chem., **621**, 1153 (1995).
- ⁶¹ M.Wörle and R.Nesper, J. Alloys Comp., **216**, 75 (1994).
- ⁶² R.Asokamani and R.Manjula, Phys. Rev. B, **38**, 4217 (1989).
- ⁶³ S.Nishimoto, M.Takahashi and Y.Ohta, Physica B, **281 & 282**, 953 (2000).
- ⁶⁴ H.Takaki, R.J.Cava, H.Eisaki, J.O.Lee, K.Mizuhashi, B.Batlogg, S.Uchida, J.Jikrajewski and W.F.Peck Jr., Physical C, **228**, 389 (1994).
- ⁶⁵ W.H.Butler, Treaties on Materials Sci. and Technol, Edited by F.Y.Fradin, Academic Press. Inc. **21**, 165 (1981).
- ⁶⁶ M.Ohashi, S.Yamanaka and M.Hattori, J. Ceram. Soc. Jpn., Ind. Edn. **97**, 1175 (1989).
- ⁶⁷ H.Ledbetter, Physica C, **235-240** 1325 (1994).
- ⁶⁸ W.L.Mcmillan, Phys. Rev. **167**, 331 (1967).
- ⁶⁹ T. Yildirim, O. Gülseren, J.W. Lynn, C.M. Brown, T.J. Udovic, H.Z. Qing, N. Rogado, K.A. Regan, M.A. Hayward, J.S. Slusky, T. He, M.K. Haas, P. Khalifah, K. Inumaru and R.J. Cava, Preprint, cond-mat/0103469 (2001).
- ⁷⁰ A.Y. Liu, I.I. Mazin and J. Kortus, Preprint, cond-mat/0103570 (2001).
- ⁷¹ D. Kaczorowski, A.J. Zaleski, O.J. Zogal and J. Klamut, Preprint, cond-mat/0103571 (2001)
- ⁷² S.Shin, A.Agai, M.Watanabe, M.Fujisawa, Y.Tazuka, T.Ishi, K.Kobayashi, A.Fujimori and H.Takagi, Phys. Rev. B, **52**, 15082 (1995).
- ⁷³ L.M.Mattheiss, T.Siegrist and R.J.Cava, Solid State Commun., **91**, 587 (1994).
- ⁷⁴ Ch. Walti, E.Felder, C.Degen, G.Wigger, R.Monnier, B.Delley, and H.R.Ott, Preprint, cond-mat/0102522 (2001).
- ⁷⁵ D.K.Finnemore, J.E.Ostenson, S.L.Bud'ko, V.P.Antropov and L.L. Boyer, cond-mat/0102114.
- ⁷⁶ B.Lorenz, R.L.Meng and C.W.Chu, Preprint, cond-mat/0102264 (2001).
- ⁷⁷ E. Saito, T. Taknenobu, T. Ito, Y. Iwasa, K. Prassides and T. Arima, J. Phys. Condens. Matter, **13**, L267 (2001).
- ⁷⁸ V.S.Shirley and C.M.Lederer in Hyperfine Interactions studied in Nuclear reactions and Decay", Edited by E.Karlsson and R.Wäppling, Almqvist and Wiksell International, Stockholm, Sweden (1975).
- ⁷⁹ R.Weht, A.Filippetti, and W.E.Pickett, Europhys. Lett., **48**, 320 (1999).
- ⁸⁰ P.S.Spoor, J.D.Maynard, M.J.Pan, D.J.Green and J.R.Hellmann and T.Tanaka, Appl. Phys. Lett., **70**, 1959 (1997).

- ⁸¹ A.F. Goncharov, V.V. Struzhkin, E. Gregoryanz, J. Hu, R.J. Hemley, H.K. Mao, G. Papertot, S.L. Bud'ko and P.C. Canfield, Preprint, cond-mat/0104042 (2001).
- ⁸² J.F.Nye, Physical Properties of Crystals, Oxford University Press, Oxford, (1985).
- ⁸³ W. Boas, F.K. Mackenzie in *Progress in Metal Physics* edited by B. Chalmers, Wiley Intescienc, Newyork, **2**, p.90, (195).
- ⁸⁴ R.Osborn, E.A.Goremychkin, A.I.Kolesnikov and D.G.Hinks, Preprint, cond-mat/0103064 (2001).
- ⁸⁵ P.Ravindran, L.Fast, P.A.Korzhavyi, B.Johansson, J.Wills and O.Eriksson, J. Appl. Phys., **84**, 4891 (1998).
- ⁸⁶ K.P. Bohnen, R. Heid and B. Renker, Preprint, cond-mat/0103319 (2001).
- ⁸⁷ R.K. Kremer, B.J. Gibson, K. Ahn, Preprint, cond-mat/0102432 (2001).
- ⁸⁸ Y.Wang, T. Plackowski and A. Junod, Preprint, cond-mat/0103210 (2001).

FIGURES

FIG. 1. Crystal structures of MgB_2 , MgB_2C_2 , LiBC and MgB_4 . Legends to the different kinds of atoms are given on the illustration.

FIG. 2. Band structure of MgB_2 and hypothetical B_2 in the AlB_2 -type framework. For the B_2 substructure we have used the lattice parameters of MgB_2 .

FIG. 3. Lower panel: Total and site projected DOS for MgB_2 and hypothetical B_2 obtained from the FPLMTO method. Middle panel: Angular momentum and orbital projected DOS for MgB_2 obtained from the FPLAPW method Upper panel: Crystal overlap Hamiltonian population (COHP) between Mg-Mg, Mg-B and B-B obtained from the TBLMTO method.

FIG. 4. Calculated total DOS for BeB_2 , CaB_2 , SrB_2 obtained from the FPLAPW method and that for MgB_4 , LiBC and MgB_2C_2 obtained from the TBLMTO method. For BeB_2 , CaB_2 , and SrB_2 we have assumed the AlB_2 -type structure and the optimized structural parameters.

FIG. 5. The band structure of BeB_2 , CaB_2 and SrB_2 with AlB_2 -type structure as obtained using the optimized lattice parameters.

FIG. 6. The band structure of LiBC and MgB_2C_2 as obtained with the TBLMTO method using experimental lattice parameters.

FIG. 7. Valence charge density in the (110) plane for MgB_2 . Corner atoms are Mg and the others are B. Both plots have 35 contours between 0 and 0.25 electrons/a.u.³.

FIG. 8. The variation of the total energy with unit-cell volume (lower panel) and c/a (upper panel) for MgB_2 (AlB_2 -type structure) as obtained from the FPLMTO calculations.

FIG. 9. Calculated directional-dependent (a) bulk, (b) Young's, (c) shear moduli and the characteristic temperature (d) for MgB_2 as obtained from the calculated single crystal elastic constants.

FIG. 10. The calculated optical dielectric tensor for MgB_2 obtained from with and without intraband contribution obtained from the FPLMTO calculation.

TABLES

TABLE I. Calculated lattice parameters (a and c are in Å), c/a ratio, bulk modulus (B_0 in Mbar), its pressure derivative (B'_0) and density of state at the Fermi level [$N(E_F)$ in states Ry⁻¹ f.u.⁻¹] for AlB₂-type compounds

Compound	a	c	c/a	B_0	B'_0	$N(E_F)$
BeB ₂	2.886	3.088	1.027	1.93	3.47	6.309
MgB ₂	3.080	3.532	1.147	1.50	3.50	9.98
...	1.20±0.05 ^a
...	1.39 ^b
...	1.51 ^c
...	1.47 ^d
...	1.40±0.06 ^e
CaB ₂	3.397	4.019	1.183	1.34	3.42	10.837
SrB ₂	3.456	4.193	1.213	1.05	2.28	4.732
TiB ₂	3.070	3.262	1.060	2.13	2.10	4.27

^aFrom synchrotron XRD by Prassides *et al.*³⁴.

^bHigh pressure XRD measurement by Vogt *et al.*³³.

^cCalculated from FPLAPW method by Vogt *et al.*³³.

^dCalculated from pseudopotential method by Bohnen *et al.*⁸⁶.

^eCalculated from FPLAPW method by Lao and Syassen³².

TABLE II. Average shear modulus (G_{av} in Mbar), longitudinal and transverse elastic wave velocity (ν_l , ν_k in m/s) and Debye temperature (Θ_D in K) obtained from single crystal elastic constant(Θ_D in K)

Compound	G_{av}	ν_l	ν_m	Θ_D (calc.)	Θ_D (exp.)
MgB ₂	1.146	10612	7276	1016	750±30 ^a
...	746 ^b
...	800 ^c
...	920 ^d
TiB ₂ (exp.) ^e	2.407	7061	5105	743	...

^aFrom specific heat measurements by Bud'ko *et al.*¹⁰.

^bFrom specific heat measurements by Wälti *et al.*⁷⁴.

^cFrom specific heat measurements by Kremer *et al.*⁸⁷.

^dFrom specific heat measurements by Wang *et al.*⁸⁸.

^eCalculated from the single crystal elastic constants of Spoor *et al.*⁸⁰.

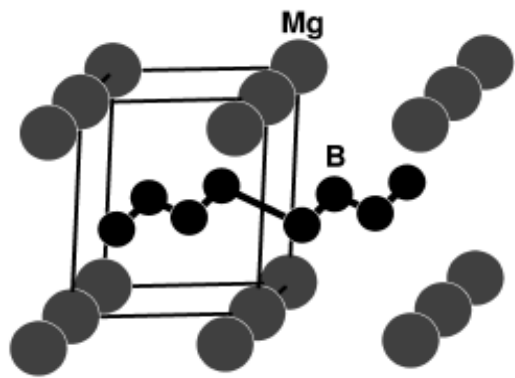
TABLE III. The single crystal elastic constants (c_{ij} in Mbar) and bulk modulus values along a and c (B_a and B_c in Mbar)

Compound	c_{11}	c_{12}	c_{13}	c_{33}	c_{44}	B_a	B_c
MgB ₂	4.380	0.430	0.329	2.640	0.802	5.406	3.006
...	4.1±0.2 ^a	2.92±0.12
...	6.25 ^b	3.33
TiB ₂ (exp.) ^c	6.6	0.48	0.93	4.32	2.6	8.512	5.527

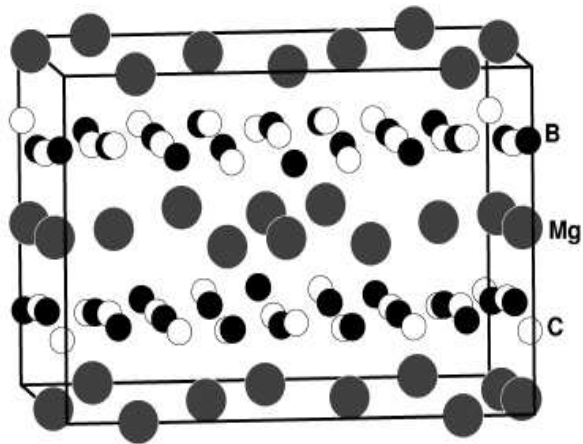
^aFrom synchrotron XRD by Prassides *et al.*³⁴.

^bFrom hydrostatic high pressure synchrotron XRD by Goncharov *et al.*⁸¹.

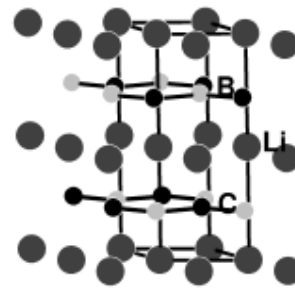
^cCalculated from the single crystal elastic constants of Spoor *et al.*⁸⁰.



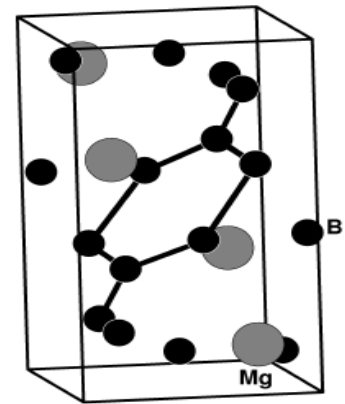
MgB₂



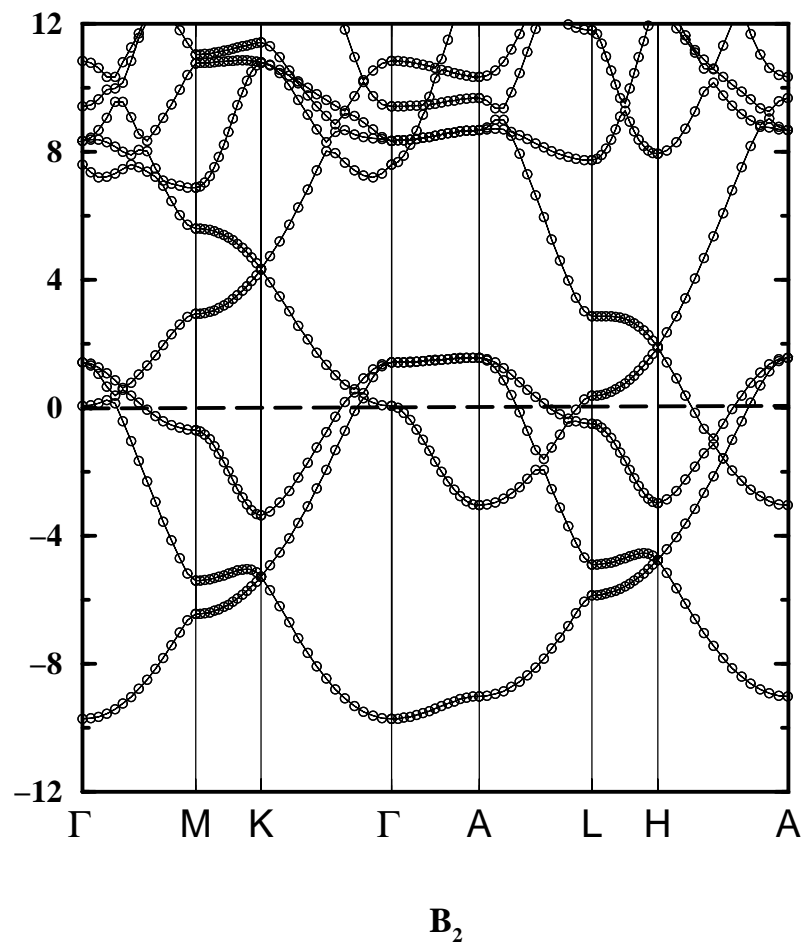
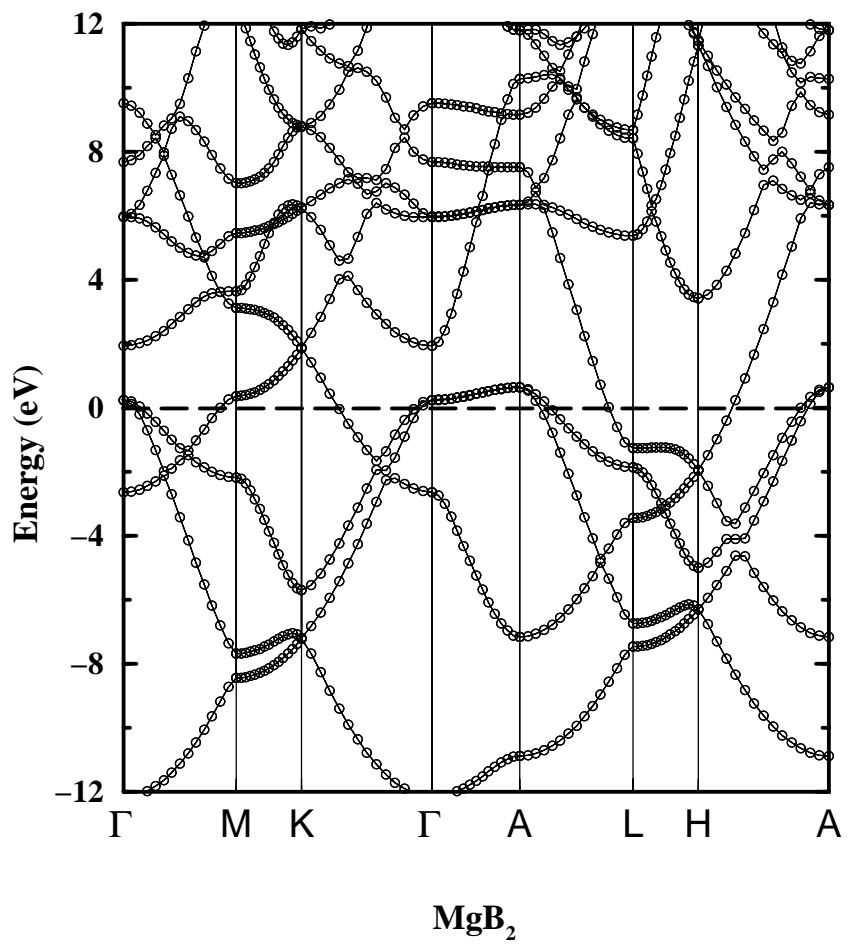
MgB₂C₂

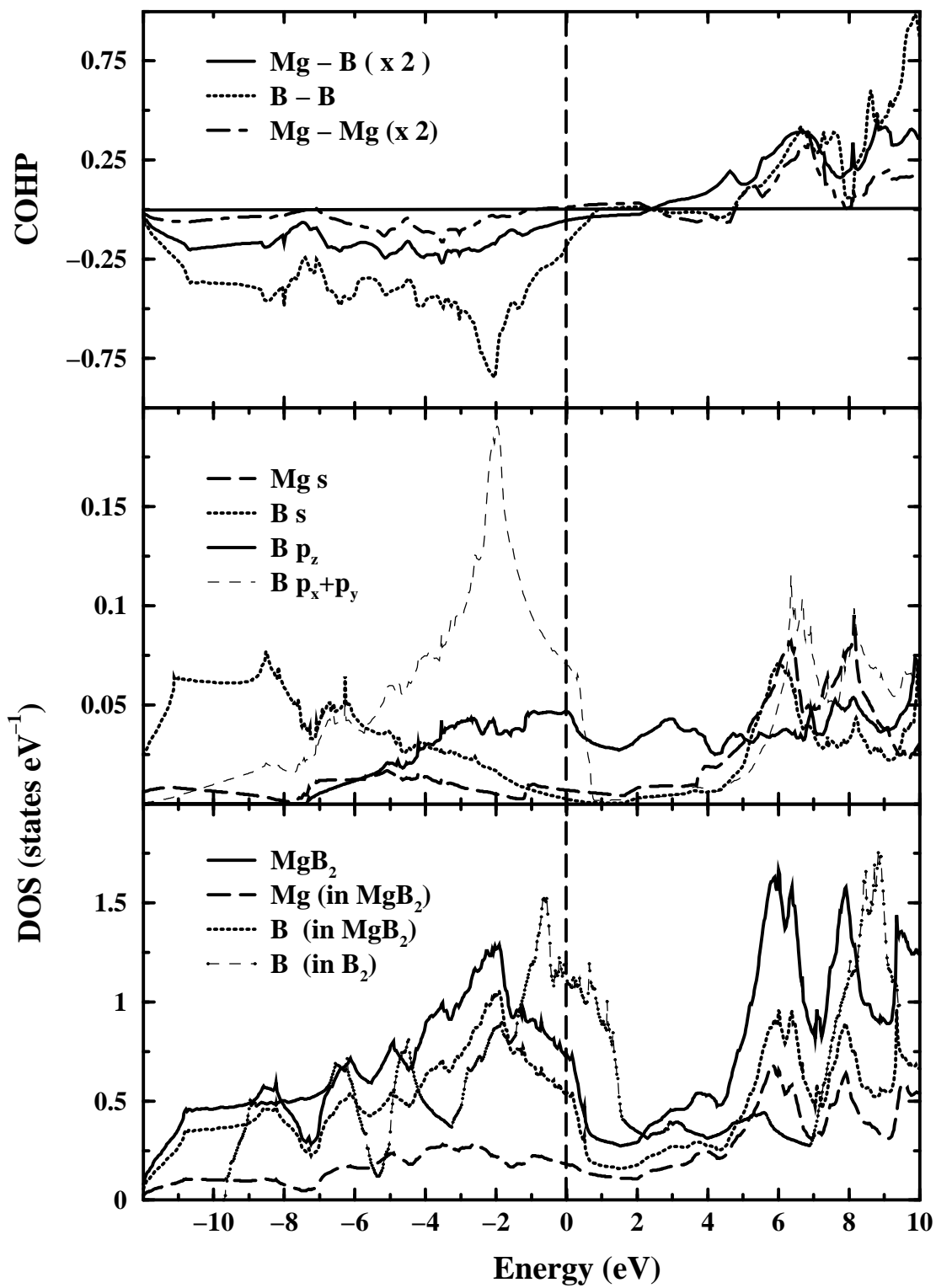


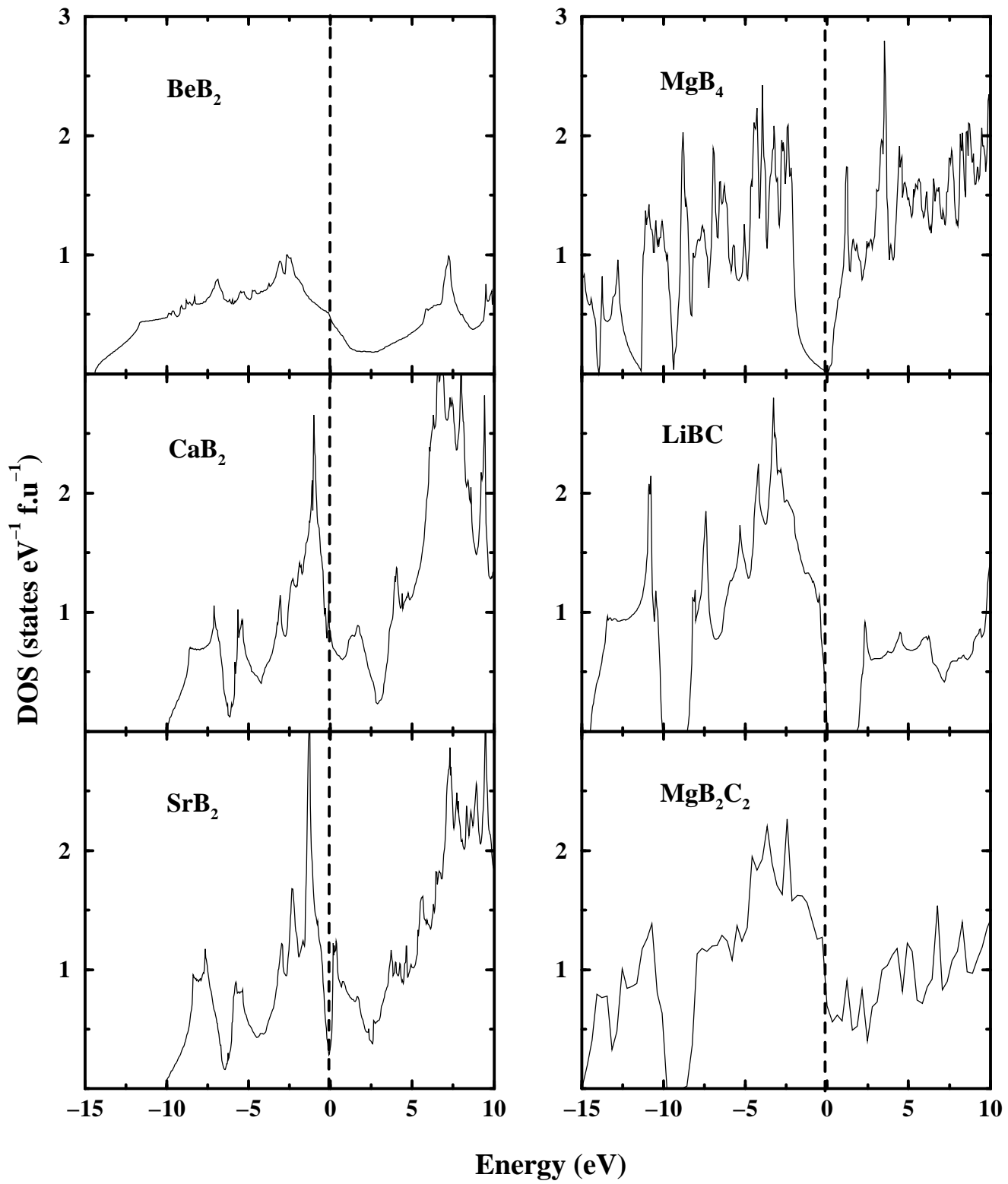
LiBC

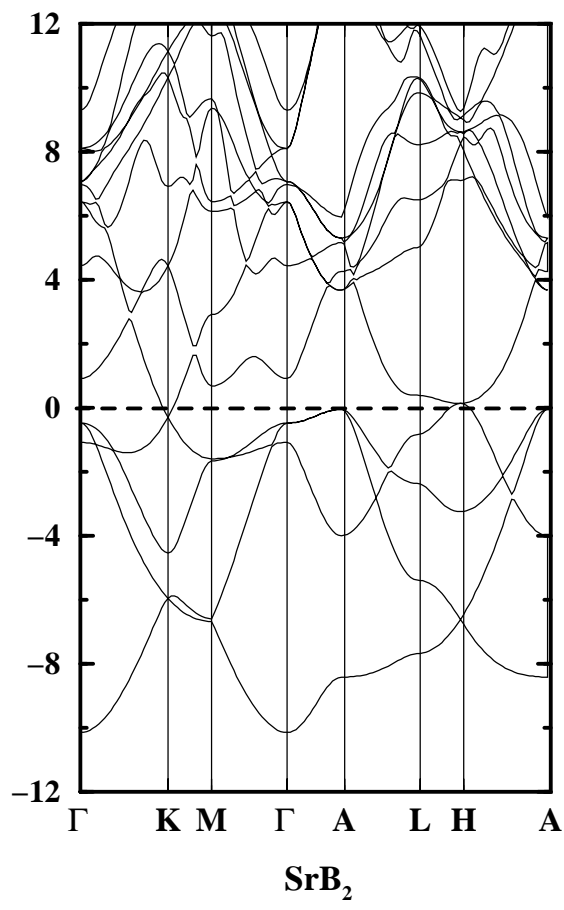
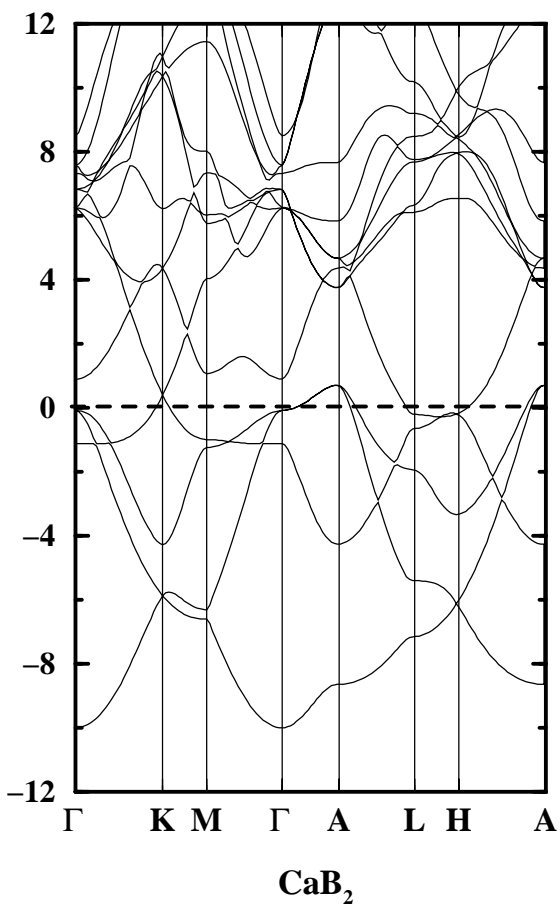
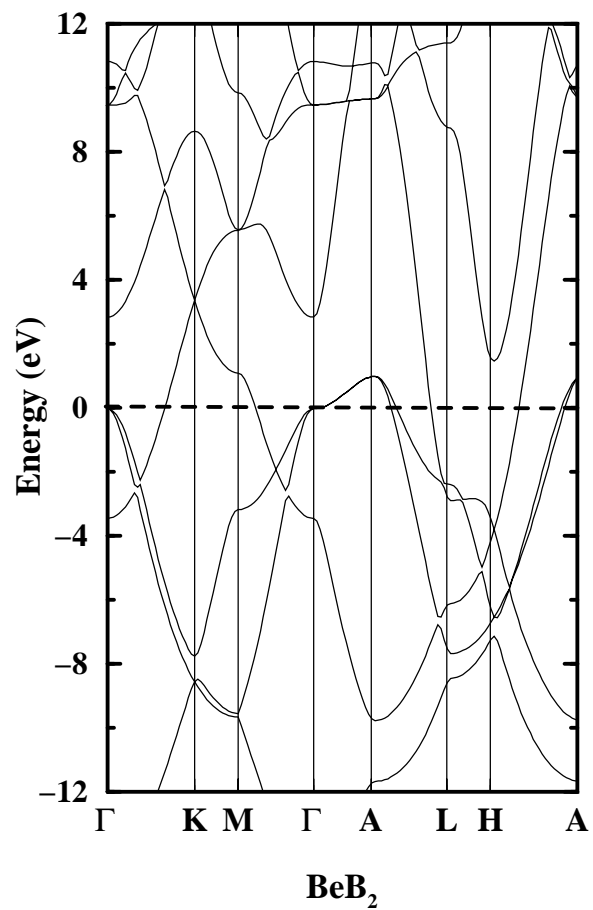


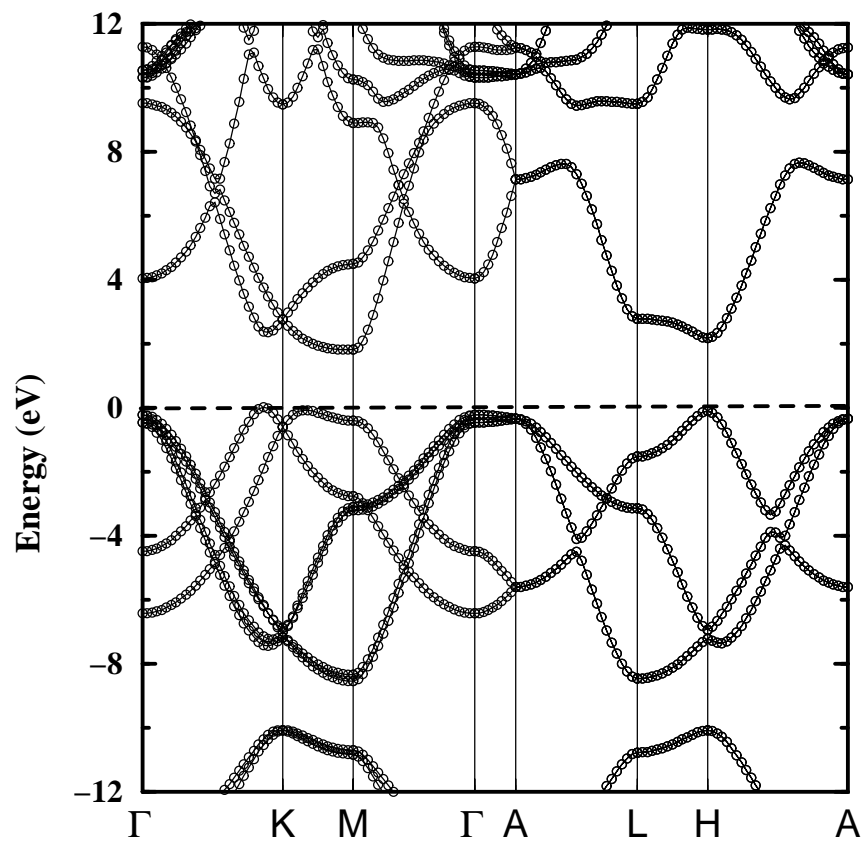
MgB₄



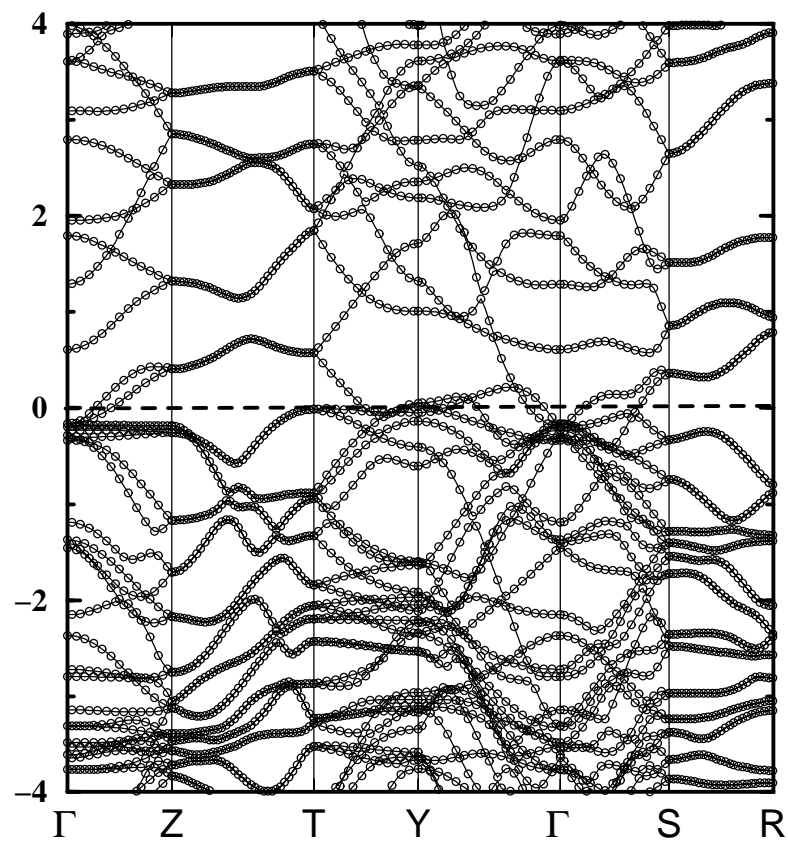




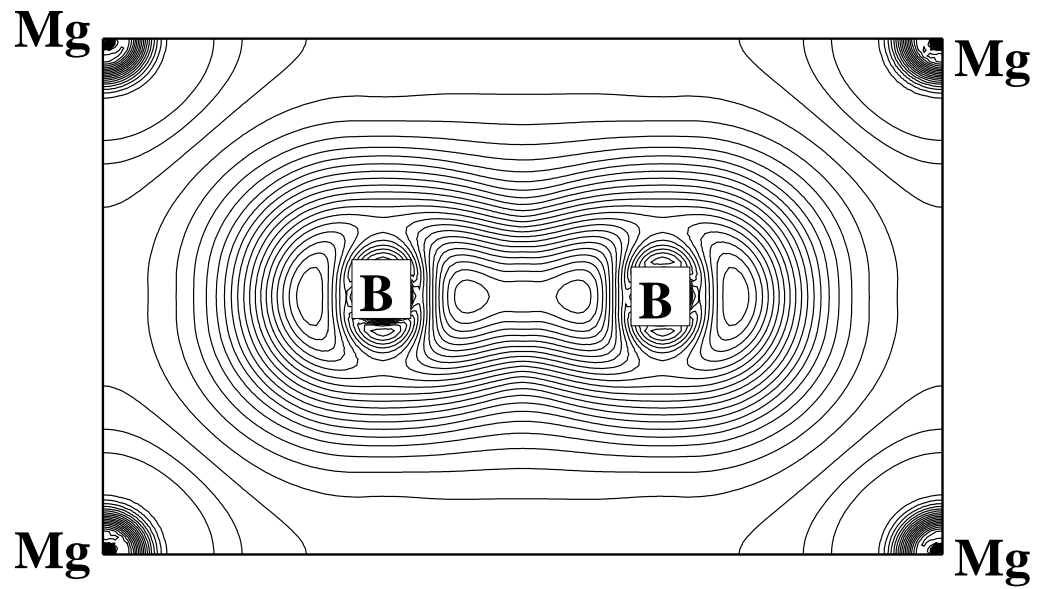
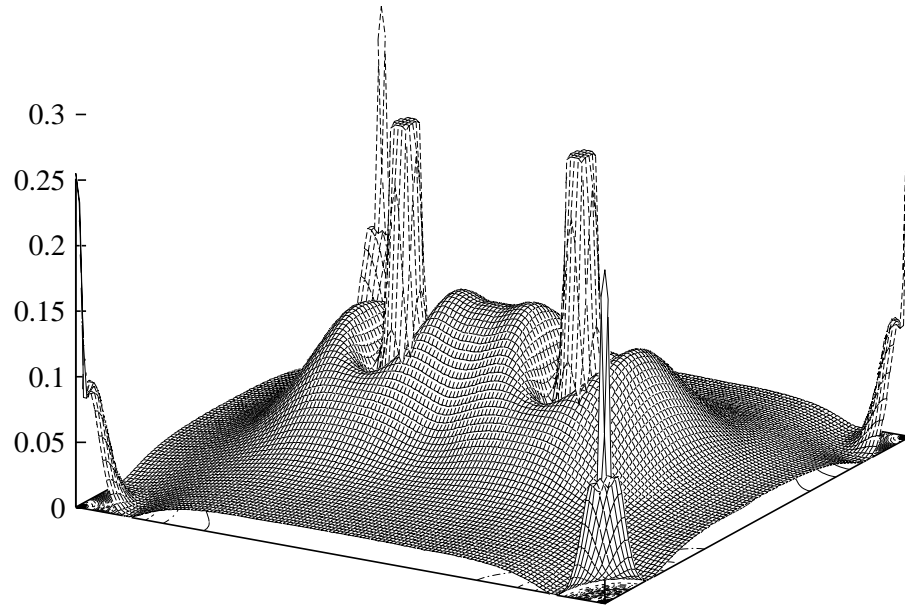


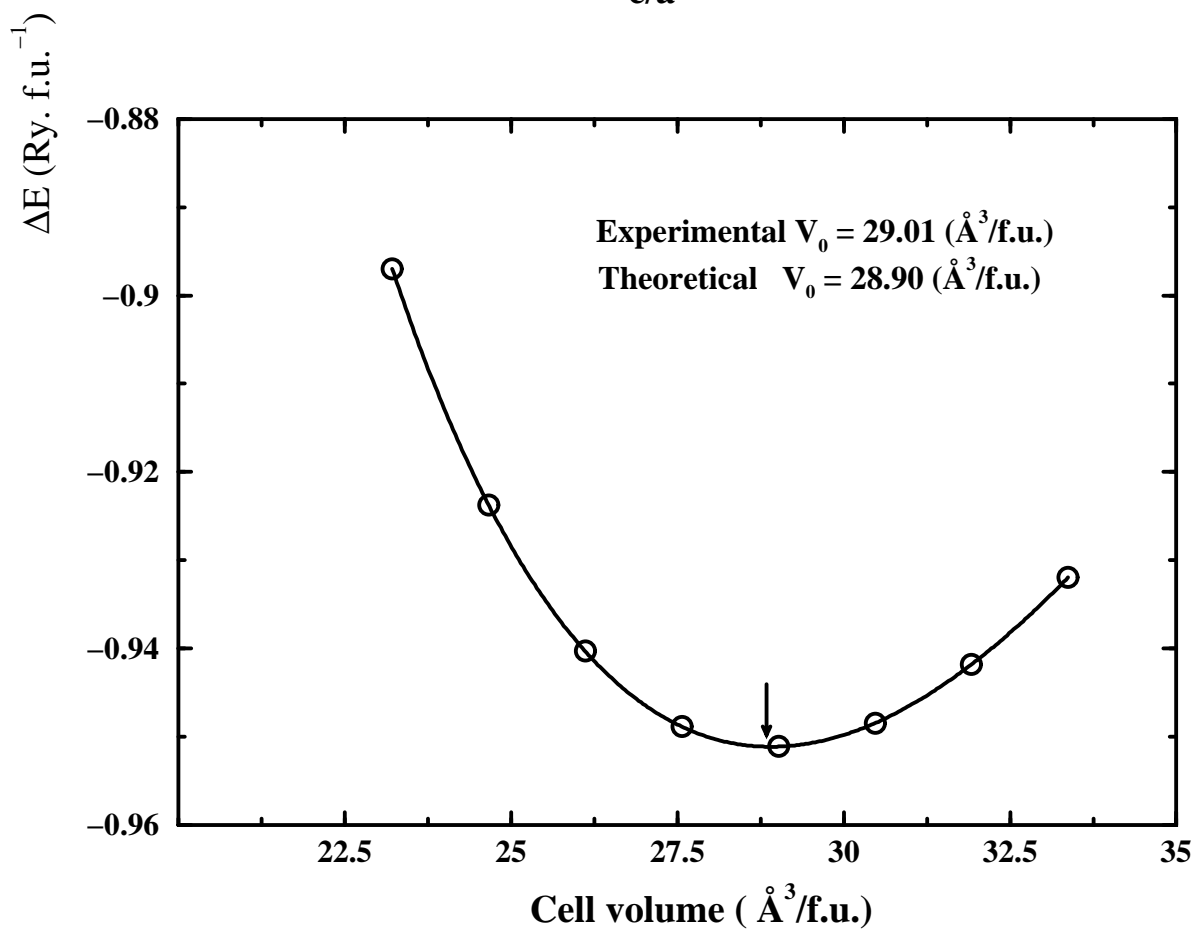
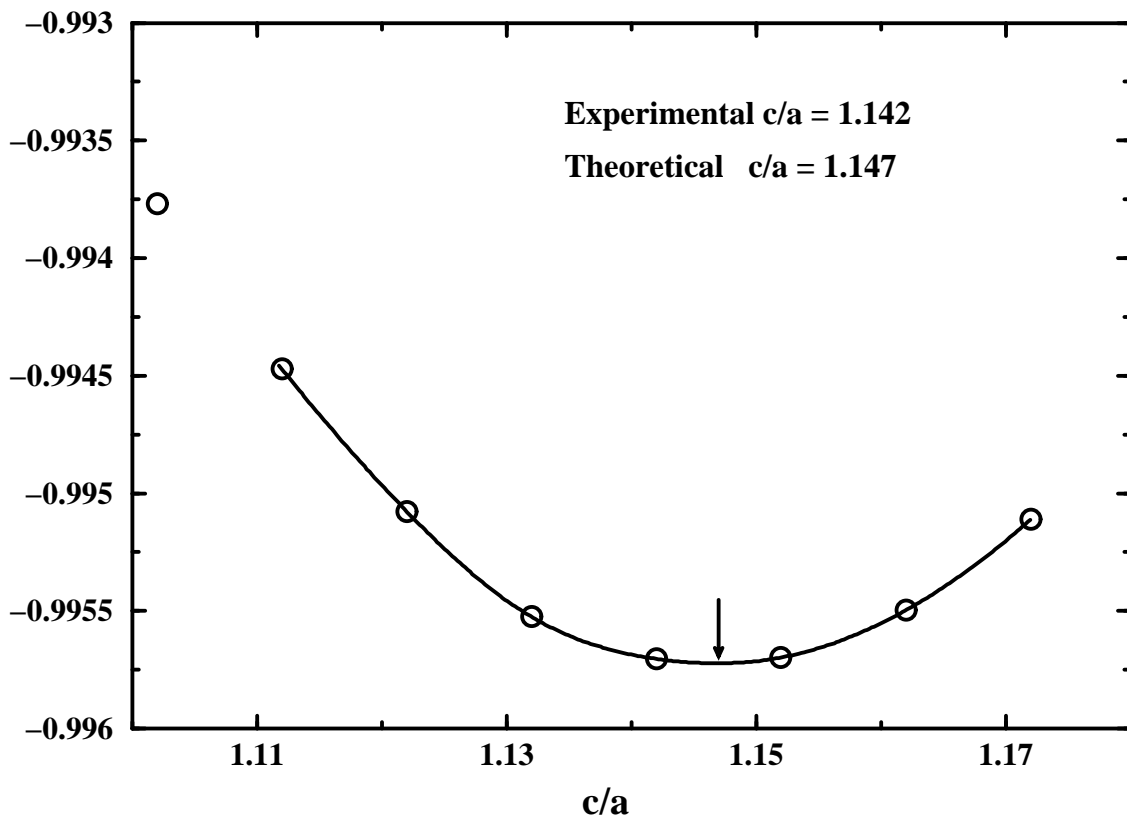


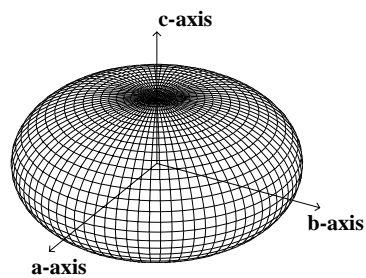
LiBC



MgB_2C_2

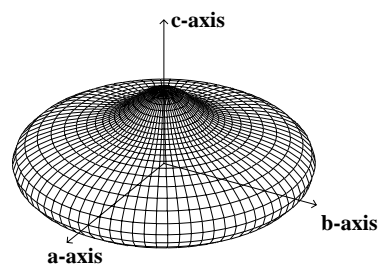






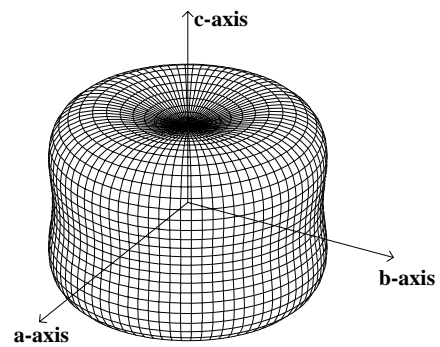
Intercepts
a-axis: 5.360 Mbar
c-axis : 3.019 Mbar

(a)



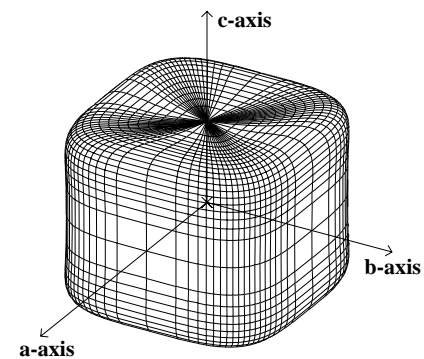
Intercepts
a-axis: 4.303 Mbar
c-axis: 2.595 Mbar

(b)



Intercepts
a-axis: 1.140 Mbar
c-axis: 0.802 Mbar

(c)



Intercepts
a-axis: 1020 K
c-axis: 850 K

(d)

